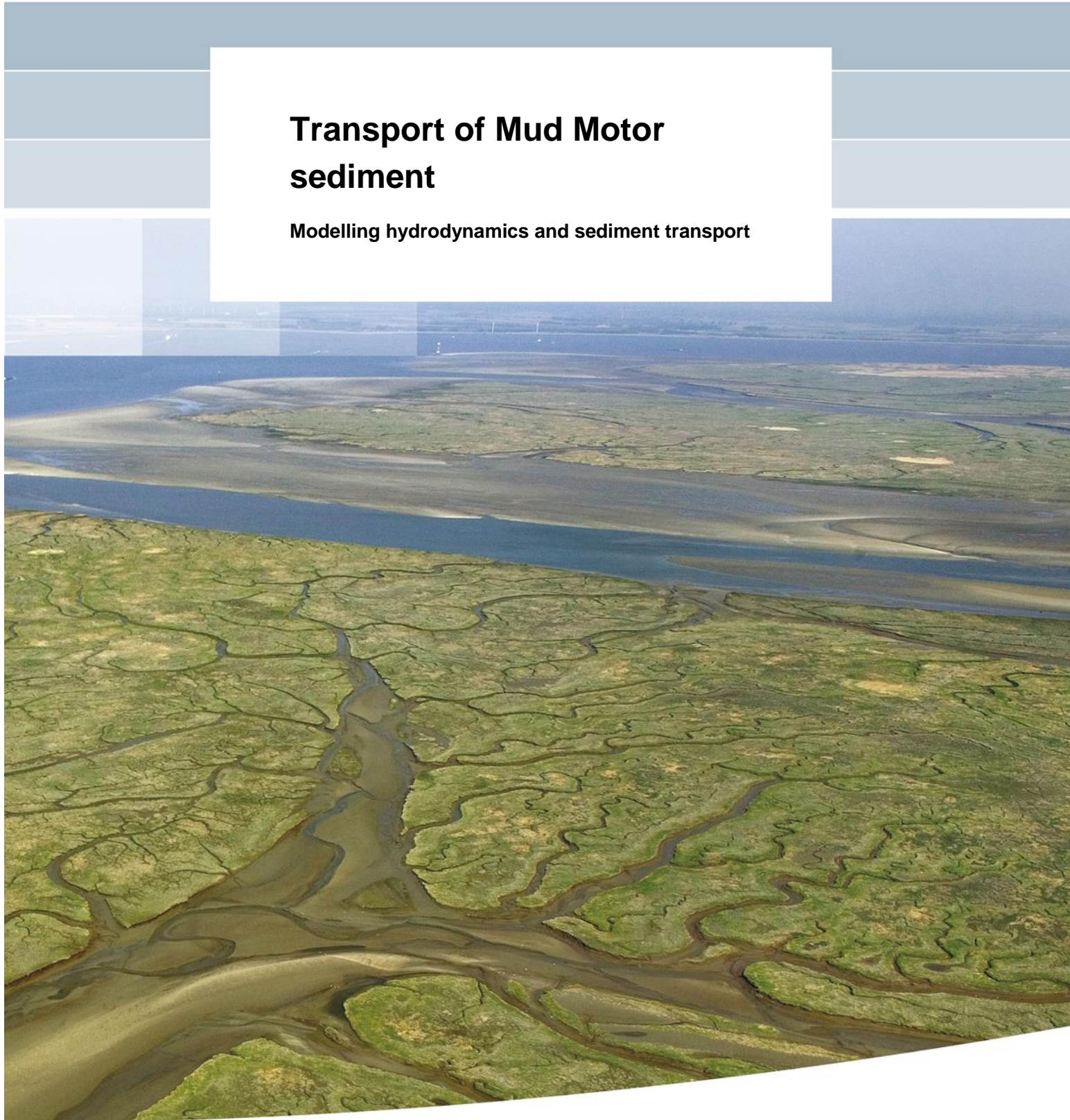# Transport of Mud Motor sediment

Modelling hydrodynamics and sediment transport

Transport of Mud Motor sediment

Modelling hydrodynamics and sediment transport

R. van Weerdenburg
J. Vroom
B. van Maren

Deltares

Title
Transport of Mud Motor sediment

Project	**Attribute**	**Pages**
1209751-012	1209751-012-ZKS-0002	35

Keywords
Mud Motor, Harlingen, fine sediment transport, sediment disposal, modelling, beneficial use of dredged sediment, Building with Nature, Delft3D-FM, mudflats, Koehoal

Summary
The mudflat of Koehoal is the intertidal area where the Mud Motor sediment disposal should contribute to salt march expansion. Field observations have already provided insight into the sediment concentrations and transport rates near this mudflat. Sediment transport rates were particularly high during north and north-eastern wind events. This led to the hypothesis that residual sediment transports are directed from the disposal area in the Kimstergat channel onto the intertidal mudflats north of the Koehoal mudflat, where sediment is temporarily stored. At the mudflats, sediment transport and redistribution are strongly governed by wind driven flows and wave resuspension, leading to residual transports towards the Koehoal mudflat during north and north-eastern wind events.

In this project the Mud Motor sediment disposal has been studied using a numerical simulation model. A newly developed model of the Dutch Wadden Sea in the Delft3D Flexible Mesh Suite was used. The only source of sediment in model simulations is the Mud Motor disposal. This implies that sediment transports from the disposal location to surrounding areas can be studied without effects of other sediment sources and of already present material at the bed. Model results show that sediment is partly transported directly from the Kimstergat channel to the Koehoal mudflat. Another part is transported to mudflats further north and east. During winds from the north and the east there is a residual transport from the northern mudflats towards the Koehoal mudflat, such that there is also an indirect transport from the Kimstergat channel to the Koehoal mudflat.

Model results also suggest that large suspended sediment concentrations that were measured at the Koehoal mudflat during north-eastern winds might be dependent on different sediment sources than the Mud Motor disposal or the Kimstergat channel. The fate of disposed sediment is strongly influenced by the sediment properties, since two sediment fractions with different settlings velocities are transported to different areas. The finer fraction appears to be more susceptible to residual flow. Upscaling of the model results to the Mud Motor pilot project in the field would imply that approximately 1.5 cm of consolidated material is deposited at the Koehoal mudflat. This agrees with earlier estimates from the tracer experiment and the LiDAR surveys, in which no large bed level changes were detected.

Version	Date	Author	Initials	Review	Initials	Approval	Initials
1.0	Oct. 2019	R. van Weerdenburg	RvW	T. van Kessel	TvK	F. Hoozemans	
		J. Vroom					
		B. van Maren					

Status
final

Contents

Deltares

1 Introduction

The field campaigns setup to monitor the effect of the Mud Motor have provided insight into the hydrodynamics and the sediment transport in the Mud Motor study area. The tracer experiment showed that the travel time from the disposal location to the intertidal / target area is in the order of a week to a month, i.e. longer than one tidal cycle (with an estimated tidal excursion length of ~10 km). Detailed flow and suspended sediment concentrations (SSC) measurements at the tidal flats show the effect of wind on the flow velocity in very shallow water on a muddy tidal flat and the relation between wind driven flow and wave resuspension and SSC. SSC was highest during winds from the NE (much higher than during comparable wind velocities from the SW), suggesting large sediment availability NE of the study site.

Earlier model work (Vroom, 2015), using a simple and local numerical model) suggested that sediment transport in the Kimstergat channel (the tidal channel draining the Koehoal tidal flat) is primarily in the along-channel direction. Therefore, the cross-shore distance of the disposal location should be minimized in order to have the sediment deposited as close as possible to the salt marshes of Koehoal. Sedimentation did not reach the high part of the intertidal area, nor the salt marshes, possibly because of absence of wind and waves, and because of relatively short simulation time.

Combining this observational data and earlier model findings leads to the following hypothesis: sediment disposed at the Mud Motor location in the Kimstergat channel, is transported in flood direction by the flood dominant tidal flow in the Kimstergat channel. At the end of the Kimstergat channel, large tidal flats are present, where the Mud Motor sediments can (temporarily) be stored. During moderate to strong wind conditions, sediments are resuspended and transported in various directions, depending on the wind direction and the tide. As the largest tidal flats lie north and east of our study area, most sediment transport towards the study area occurs during winds from the north and the northeast.

In order to test this hypothesis, a numerical model (including wind and waves) has been set-up. to test if sediment is transported in the way as described above. Moreover, this numerical model gives insight in the sediment transport outside the areas that have been monitored extensively, i.e. the larger tidal flat area ('Terschellinger Wad', 'Ballastplaat', see Figure 1.1), the Kimstergat and the coast between Harlingen and Zwarte Haan.
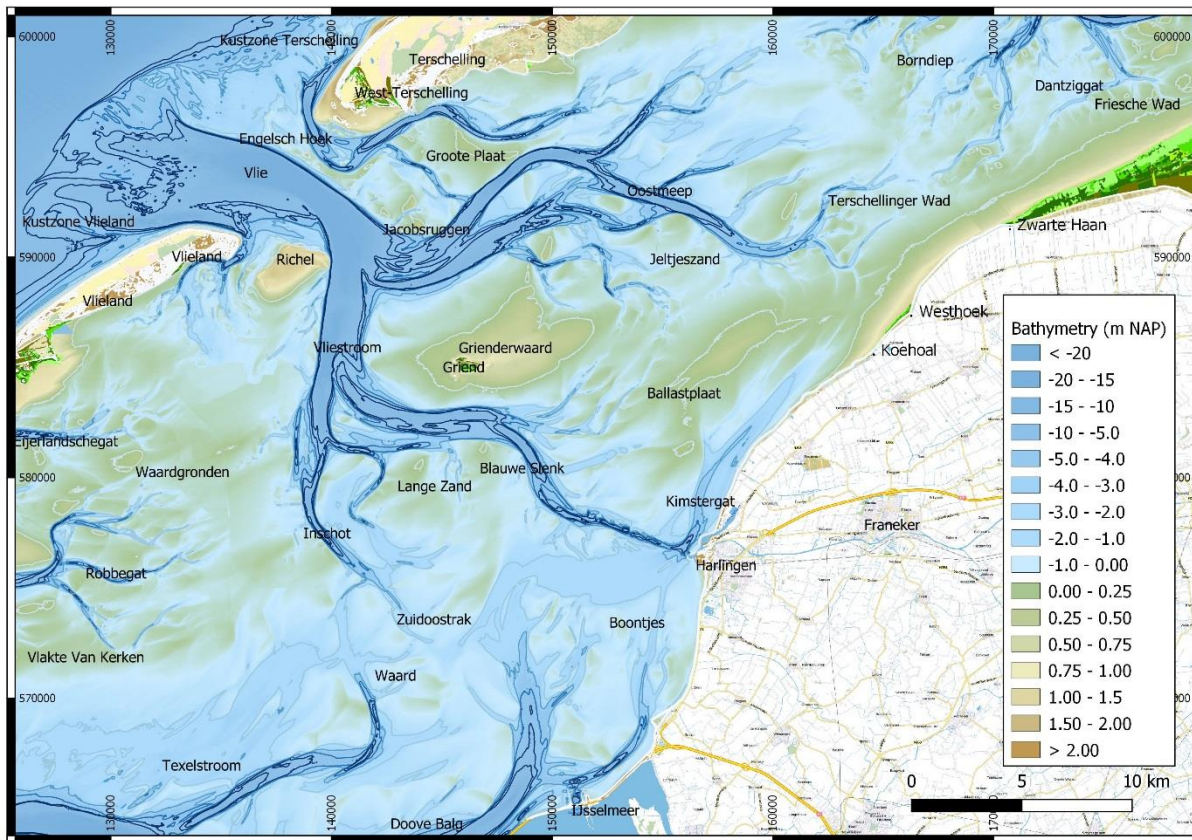
Figure 1.1 Map with names of intertidal flats, channels and salt marsh location in the area of interest. Bathymetry from 2010. The Mud Motor salt marsh is situated between Koehoal and Westhoek. Bright green colour (not in the colour map) indicates vegetation. Taken from Baptist et al. (2019).

2 Hydrodynamic model

2.1 Model set-up

The hydrodynamics are computed with the co-called Delft3D-Flexible Mesh 3D Dutch Wadden Sea Model (DWSM). The model development is part of a more comprehensive project in which sixth-generation hydrodynamic models are developed for many Dutch water bodies maintained by Rijkswaterstaat. Eventually, the DWSM model will be in 'beheer & onderhoud' ('management & maintenance') for Rijkswaterstaat. This implies that the grid design is based on several standards and calibration of the water levels is done by adjusting the bottom roughness via an automated data assimilation procedure (called OpenDA-DUD) (Zijl et al., 2016). Also, the bathymetry and features in the model domain (cross-shore groins, dams and dry points) are derived from Baseline, to secure reproducibility of the files.

The DWSM model covers the entire Dutch Wadden Sea including the Ems estuary (see Figure 2.1). The western, northern, eastern and southern offshore boundaries are located at 4° E, 53.975° N, 7.3875° E and 52.55° N, respectively. The latter being just north of the port of IJmuiden. The grid resolution of the hydrodynamic model is 0.5 nautical mile ('nm') x 0.5 nm at the coarsest area in the northwestern corner of the model domain. The model resolution increases in 3 steps to around 100 m x 100 m (i.e. 1/16 nm, to be more precise) for the Wadden Sea and the North Sea coast, to accurately include the tidal inlets and ebb-tidal deltas.

The water column is discretized by using 20 σ-layers in the hydrodynamic model. This high resolution in the vertical direction allows for accurate representation of salinity and water temperature gradients – and related processes – in the hydrodynamic model. The model is forced by water level, 3D salinity and 3D water temperature timeseries at the four offshore boundaries. These timeseries are derived from the 3D 0.5 nm Dutch Continental Shelf model (DCSM) by nesting. Freshwater discharges into the model domain are included by timeseries for sluices at Den Oever, Kornwerderzand and Lauwersoog and at the upstream end of the Ems river. The model has been set-up for the year 2016, which is the period for which we have detailed tidal flat measurements.

The model bathymetry near the location of the Mud Motor is shown in Figure 2.2. This bathymetry is based on the Vaklodingen dataset from 2009-2014 (and 2010 in the Vlie basin and hence the study area) as included in Baseline. The atmospheric forcing mechanisms are based on KNMI HIRLAM model data (i.e. air pressure, wind speed, wind direction, dewpoint, air temperature and cloudiness).
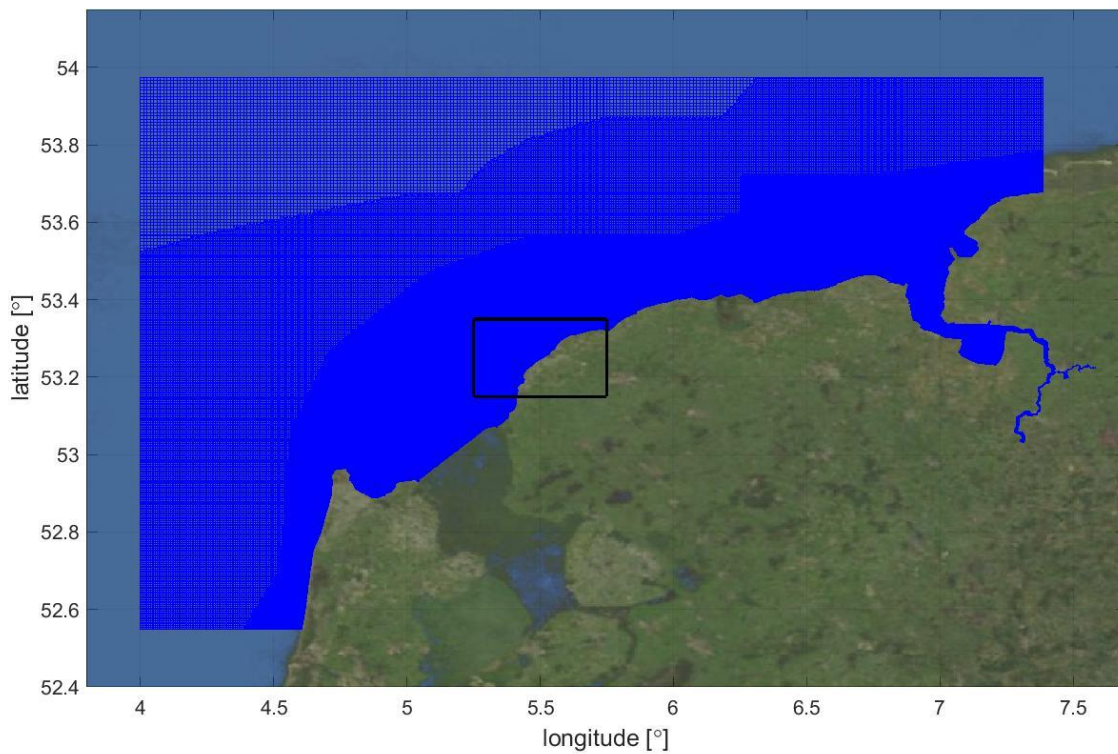
Figure 2.1   Computational grid and thereby the model domain of the 3D hydrodynamic Dutch Wadden Sea Model in Delft3D-Flexible Mesh. Areas with different resolutions are distinguished by intensity of the blue color. The black box indicates the area included in Figure 2.2.
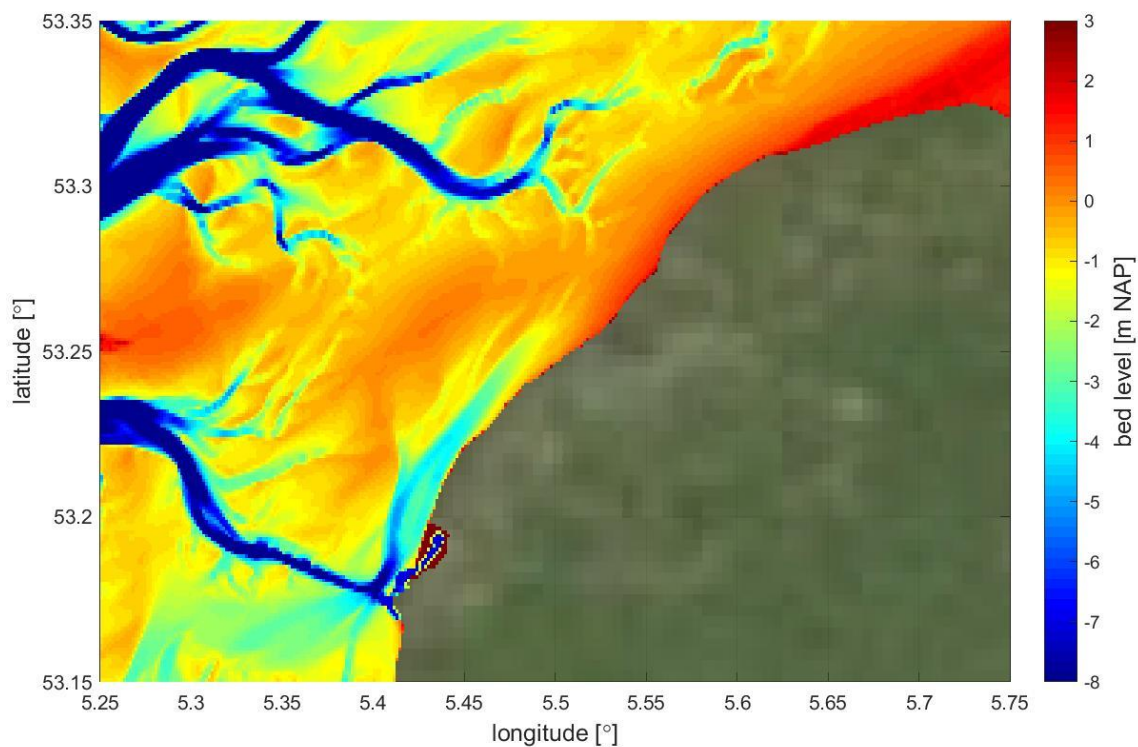

Figure 2.2   Model bathymetry near the location of the Mud Motor. The model bathymetry is generated using the Baseline software. The bed elevation is relative to NAP.

During the calibration of the 6th generation hydro software the Manning bed roughness coefficients are adjusted in order to better reproduce the measured water levels at observation points. Figure 2.3 shows the Manning roughness coefficient near the study site in the current version of the hydrodynamic Delft3D-FM model. As shown in Figure 2.3, near the study site there is a transition towards a lower Manning coefficient in the east.
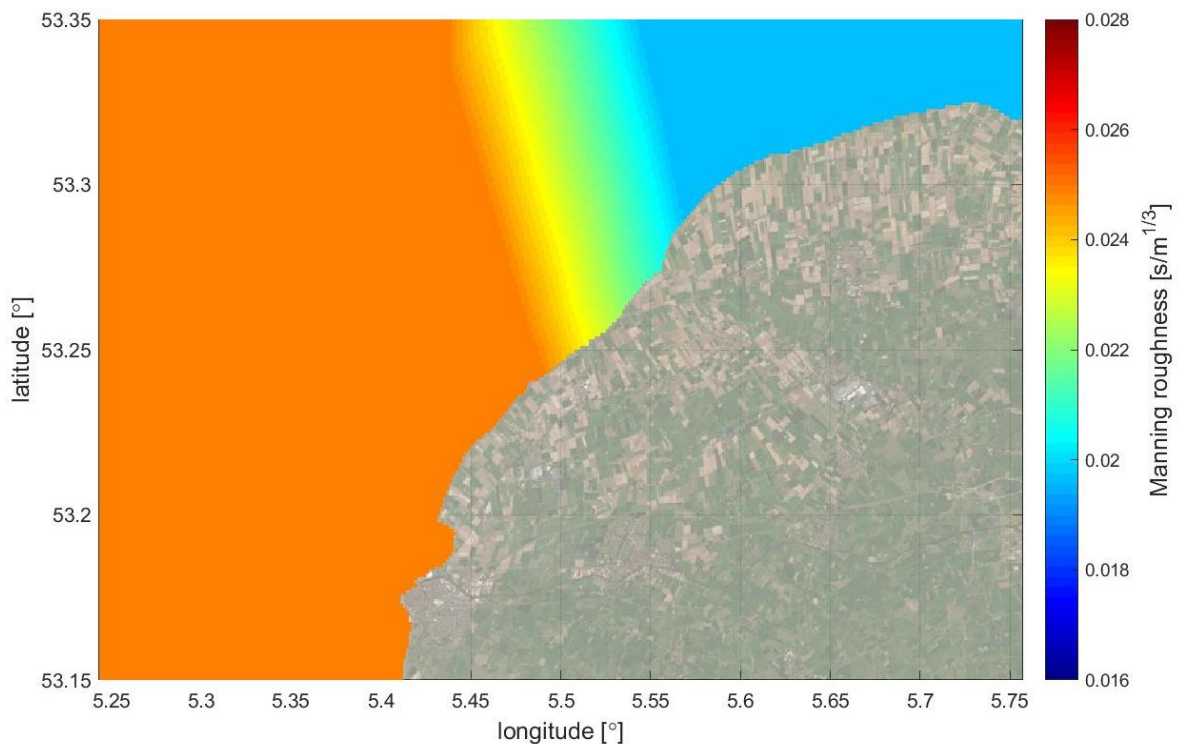

Figure 2.3   Manning roughness coefficient in the Delft3D-FM hydrodynamic simulation model.

Although this hydrodynamic model is still in development, an intermediate version of the model was considered sufficiently accurate in terms of water level reproduction for sediment modelling near Koehoal. The accuracy of the intermediate version of the DWSM model is discussed in the following section.

2.2   Validation

Two different sets of field observations are used for the validation of the hydrodynamic model for use in this study. The first set consists of water levels at measurement stations in both the North Sea and the Wadden Sea. The second set consists of measured water levels and flow velocities during the Mud Motor field campaign in April and May 2016.

For the model performance in predicting the water levels, the model results are compared with measured timeseries at stations of Rijkswaterstaat. To objectively evaluate the model performance, the unbiased RMSE is computed. The bias of a few centimeters is partly caused by using a combination of different reference levels; water level boundaries are relative to mean sea level (MSL), whereas the bathymetry and observed timeseries are relative to NAP.

The unbiased RMSE at water level gauges in the Wadden Sea is shown in Figure 2.4 for the period of interest (April 10th 2016 – May 25th 2016). At most stations, the unbiased RMSE is 5-9 cm, which is very accurate for the current stage of the model setup, but even more for the purpose of this study. The predecessor of the current model, the 'PACE' model, had a resolution

of 200x200m and a different roughness formulation, z0, which was spatially uniform. With this model a RMSE of 5-26 cm was achieved at the same Rijkswaterstaat water level gauge stations. The new DWSM model is an improvement compared to this model. Further analysis of the water level timeseries at the two stations with worst results (Holwerd and AWGPFM) reveals that:

- Holwerd station is located at the end of a narrow and meandering tidal channel which cannot be represented in detail in the model bathymetry because of the grid resolution. This is mainly affecting low water levels. In our study area the channels are captured with sufficient resolution, so this is not an issue.
- computed water levels at AWGPFM are slightly out of phase with measured water levels. Since the model results at nearby stations are more satisfying, it is not sure whether the phase difference originates from an error in the measurements or from poor performance of the model at this location.
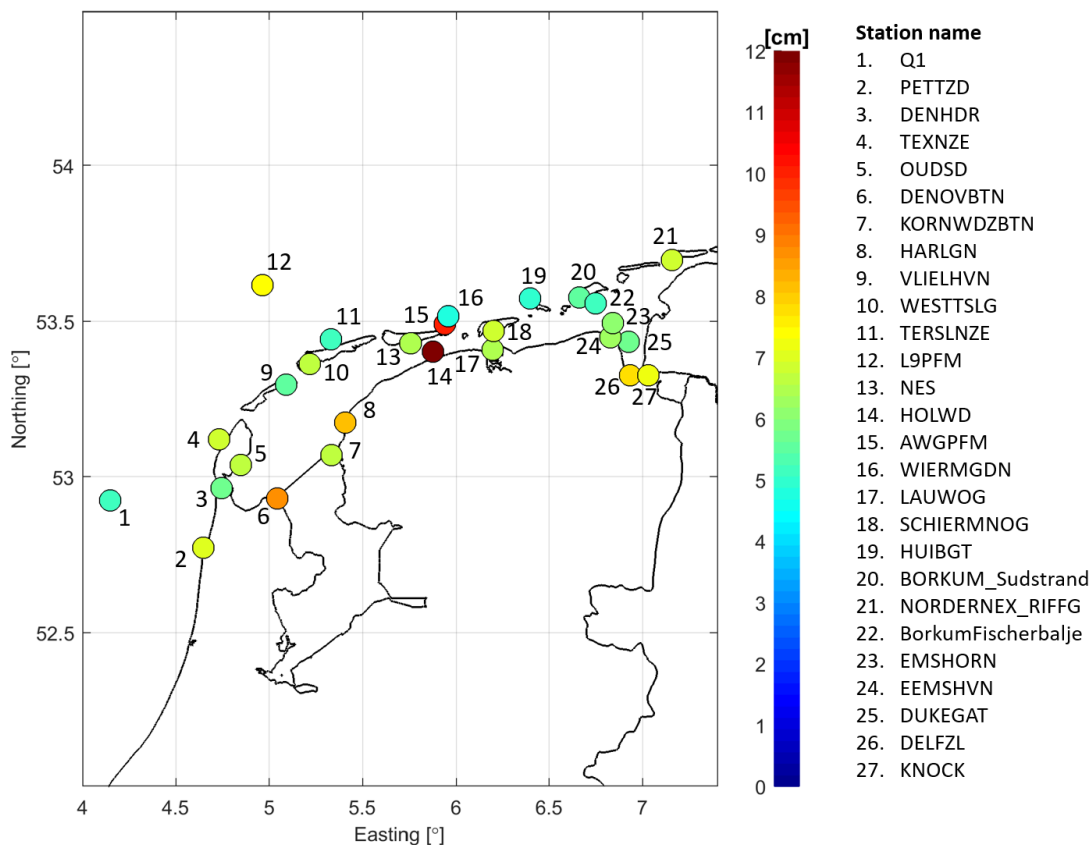

Figure 2.4   Hydrodynamic model performance in predicting the water level variability at observation points. The colour indicates the unbiased RMSE in the period April 10th – May 25th, 2016.

When we zoom in to the model performance at Harlingen, the station closest to our study area, we decomposed the water level signal in a tidal and a non-tidal signal using the t-tide toolbox, to investigate how well the model captures the effect of wind on water levels. The tidal constituents are reproduced well (Figure 2.5), both the amplitudes and the phases. The phase of the M4 constituent is 20° overestimated, introducing a small error in the main source of tidal asymmetry (the M2-M4 combination, indicated with the phase difference $2\theta_{M2} - \theta_{M4}$). The 'residual' water level signal (the original signal minus the astronomical water level as derived from the tidal analysis) contains the wind-setup or set-down (surge) and the non-resolved tidal signal. The model also reproduces this surge well, for example the wind set-up on the 15th of

May (Figure 2.6). Hence, the wind forcing on the model (KNMI HIRLAM model data which is varying in time and space) is appropriate for simulating the water level variations.

Figure 2.7 shows scatterplots of computed and observed water levels at Harlingen for both the total (tidal signal + surge) and the tidal signal. The largest mismatch between the computed and the observed water levels occurs during low water; low water levels are computed higher than observed. Overestimating the low water levels is – unfortunately – a well-known phenomenon in modelling hydrodynamics in estuarine systems with complex bathymetries. The reason is the smallest channels being not included in the model bathymetry because of insufficient grid resolution, although they are important for draining the flats towards the deeper channels. However, low water levels are better captured by the DWSM model compared to its predecessor, the PACE model.
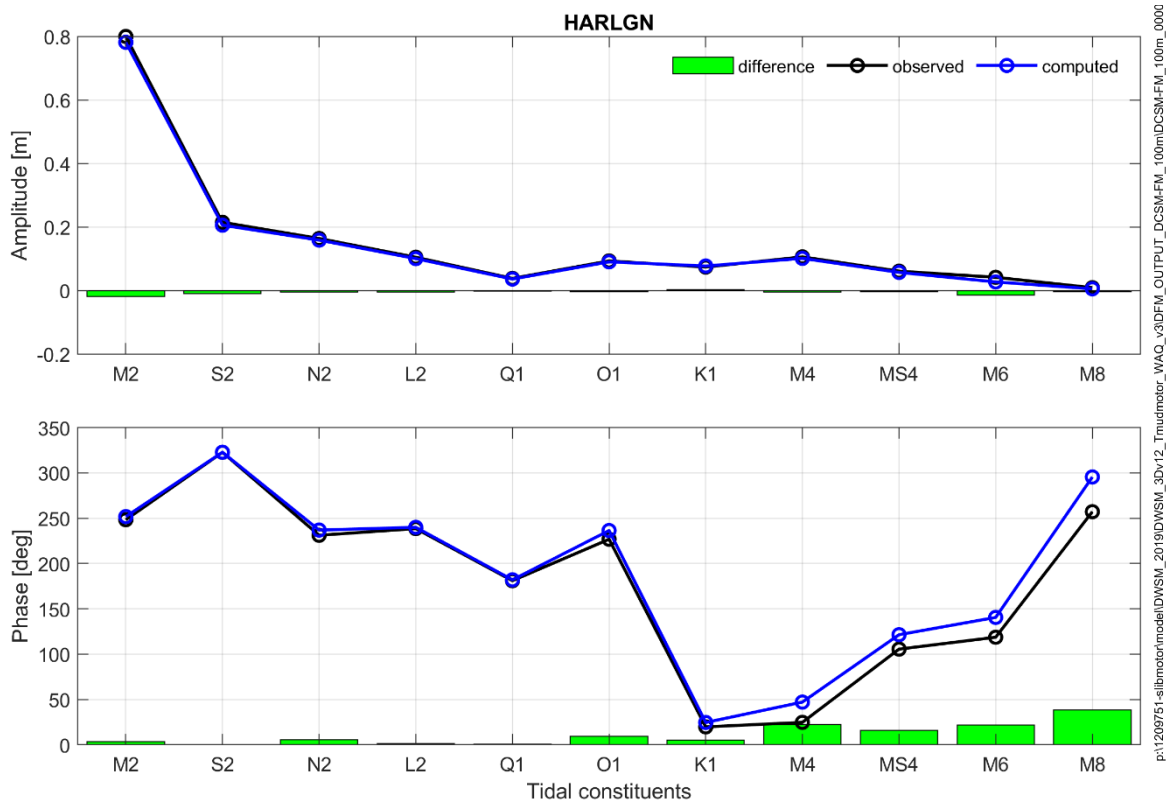

Figure 2.5   Amplitudes and phases of tidal constituents of the water level signal as observed and as computed at Harlingen.
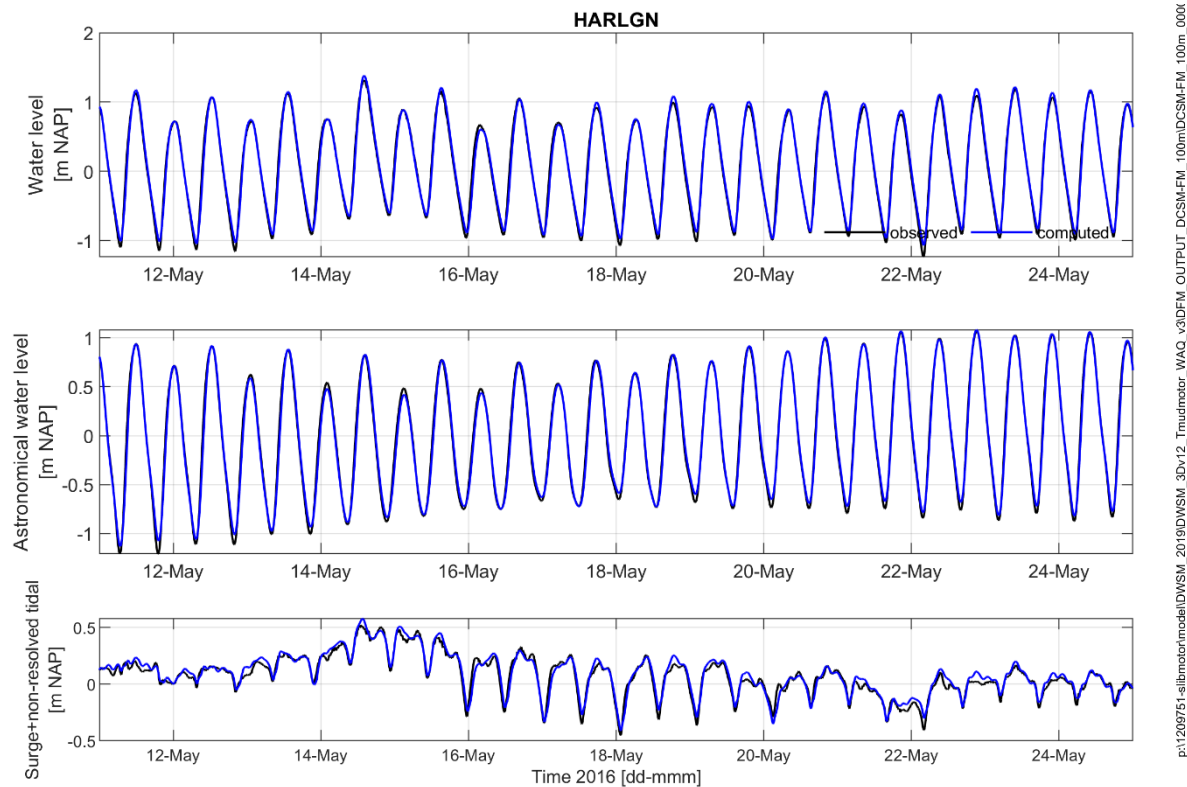
Figure 2.6   Water level timeseries as observed and as computed at Harlingen (top panel), astronomical water level (middle panel) and difference of full water level and astronomical water level, i.e. surge and non-resolved tidal signal (bottom panel).
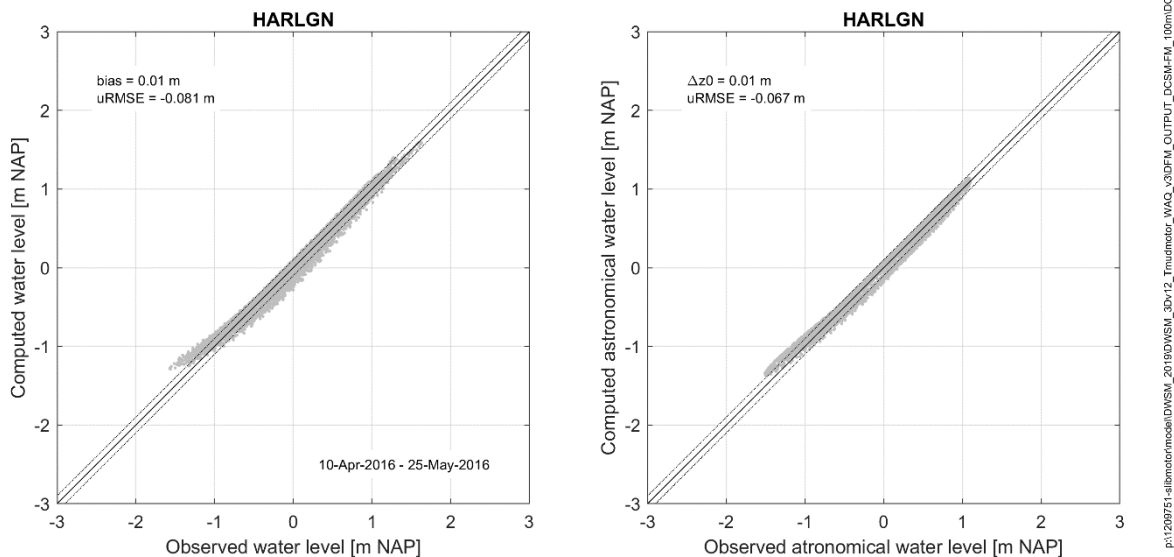

Figure 2.7   Scatter plots of water level (left) and astronomical water level (right) with computed values on the vertical axis and observed vales on the horizontal axis. In the upper left corner of the figure the bias and unbiased RMSE are given.

In April and May 2016, field measurements were carried out at an intertidal flat close to Koehoal, reported in Colosimo et al. (in review). During this field campaign timeseries of the water level and flow velocities were measured at a local observation point (5.50078° E, 53.25782° N), which is referred to as Frame 1 (lower mudflat). An ADV instrument was used to measure local

flow velocities at 20 cm above the seabed. Also, the pressure sensor of the ADV was used to determine a timeseries of the local water level.

Figure 2.8 shows timeseries of the observed and computed water levels at Frame 1 (lower mudflat) during part of the simulation period. In general, the low water levels are overestimated by the hydrodynamic model, as was also observed at Harlingen. In addition, a slightly different shape of the tidal signal leads to a relatively high unbiased RMSE of 21.5 cm. The modelled tidal water level is more asymmetric (with a shorter flood period than the data suggests), suggesting that the modelled bed roughness in the Kimstergat and nearby tidal flats are too large.
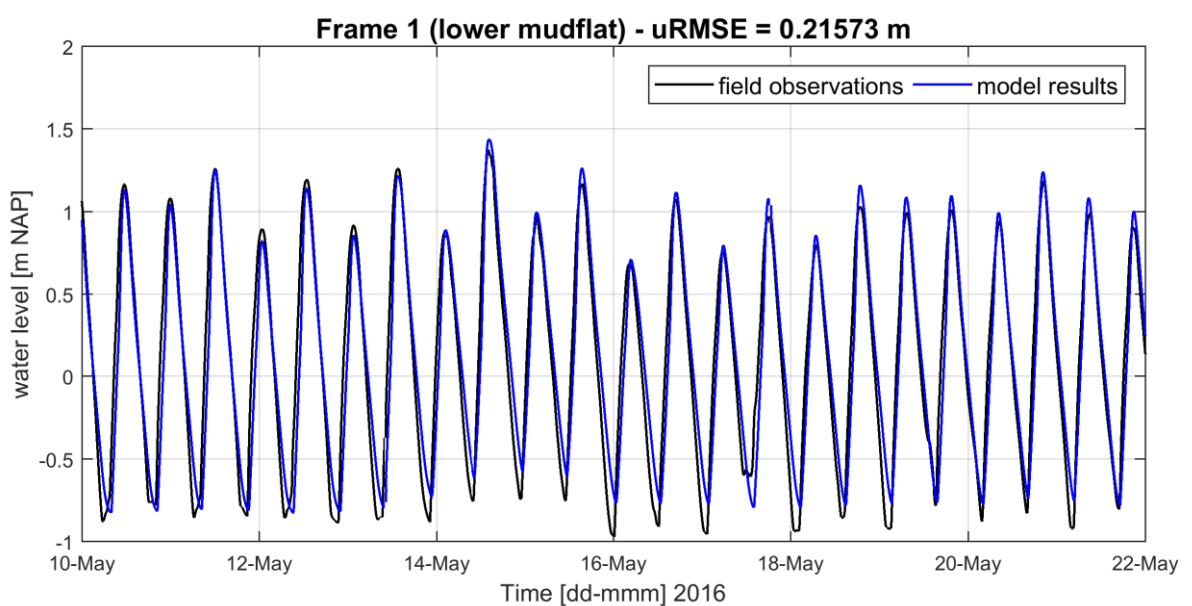

Figure 2.8   Water level computed (blue) and observed (black) at the location of Frame 1 (lower mudflat), at the mudflat near Koehoal.

Comparison of modelled and observed flow velocities is not straightforward, because the model is vertically discretized using σ -layers of which the vertical position varies with the water depth. The modelled flow velocities are therefore interpolated to 20 cm above the seabed to match the vertically constant observational data. The instantaneous flow velocities at the tidal flat are underestimated by approximately 50%, although the ebb/flood inequality is reasonably reproduced (Figure 2.9). The underestimation of the instantaneous flow velocities further suggests the bed roughness in the model is too large (supporting the apparent flood dominance of the water level). Also, the area of interest is covered with a bathymetry of 2010, which might give small deviations compared to the actual bed level in 2016. In very shallow water depths, these differences may become more important. Other modelling studies, for example from the Plaat van Walsoorden in the Western Scheldt, have also improved the computed flow velocities by tuning the bed roughness and using recent bathymetric data (Schrijvershof & de Vet, 2018).

Next, the flow velocities are tide-averaged to evaluate the relation between residual flow and wind velocity / direction. The tide average velocities are computed as the average velocity vector over an M2 period between two successive low waters. The tide averaged velocities differ from the residual flow, because the water levels are different during for example the ebb and the flood flow. The results are shown in Figure 2.11, in which the tide averaged velocities in both the field observations and the model results are shown in relation to the tide averaged

wind conditions. The tide averaged wind conditions are computed as the average of measured wind vectors during a tidal period. Since the differences in tide averaged velocities are influenced by gaps in the observations during low water levels, the data gaps are copied onto the model. In general, the variation with the wind forcing shows good correspondence with field measurements. The magnitude of the predicted tide averaged velocity is lower than observed flow velocities, similar to the instantaneous velocities were underestimated.

Improvement of the model performance with respect to flow velocities is part of the development of the model in the framework of the next generation hydro software and other (sediment) studies that build upon the same hydrodynamic model. Also, correctly reproducing low water levels and the shape of the tidal signal at intertidal areas requires more attention.
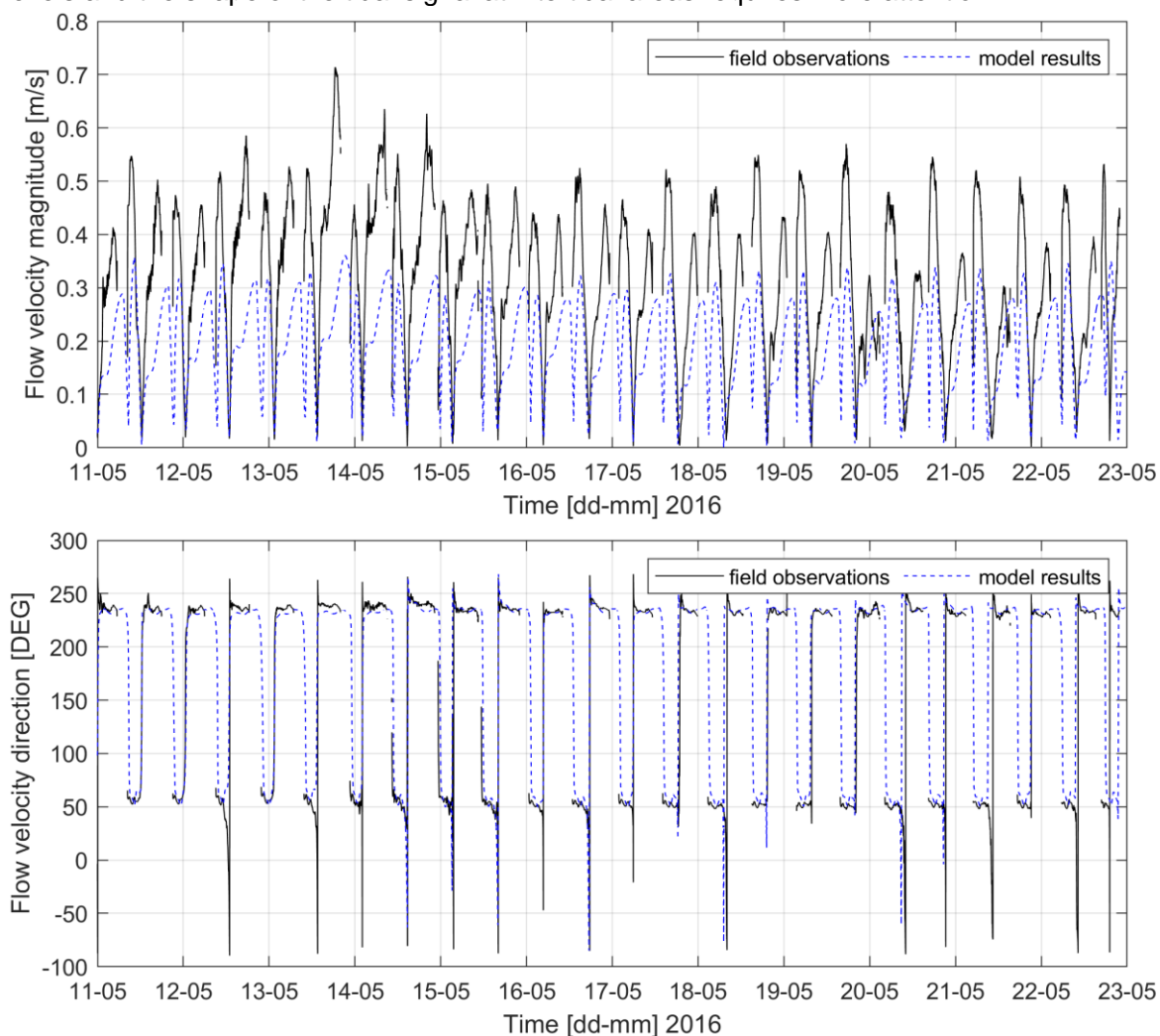
Figure 2.9   Flow velocity magnitude (top) and direction (bottom) as computed by the model (dotted blue) and as observed (black) at Frame 1 at 20 cm above the sea bed.
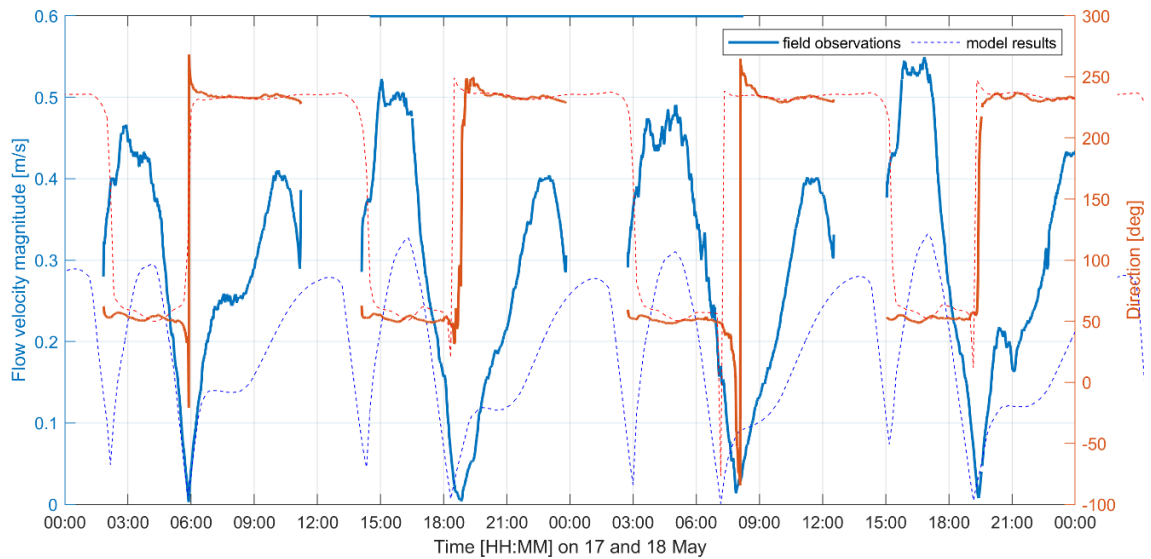
Figure 2.10 Zoom of flow velocity magnitude (left axis, blue) and direction (right axis, orange) as computed by the model (dotted) and as observed (solid) at Frame 1 at 20 cm above the sea bed.
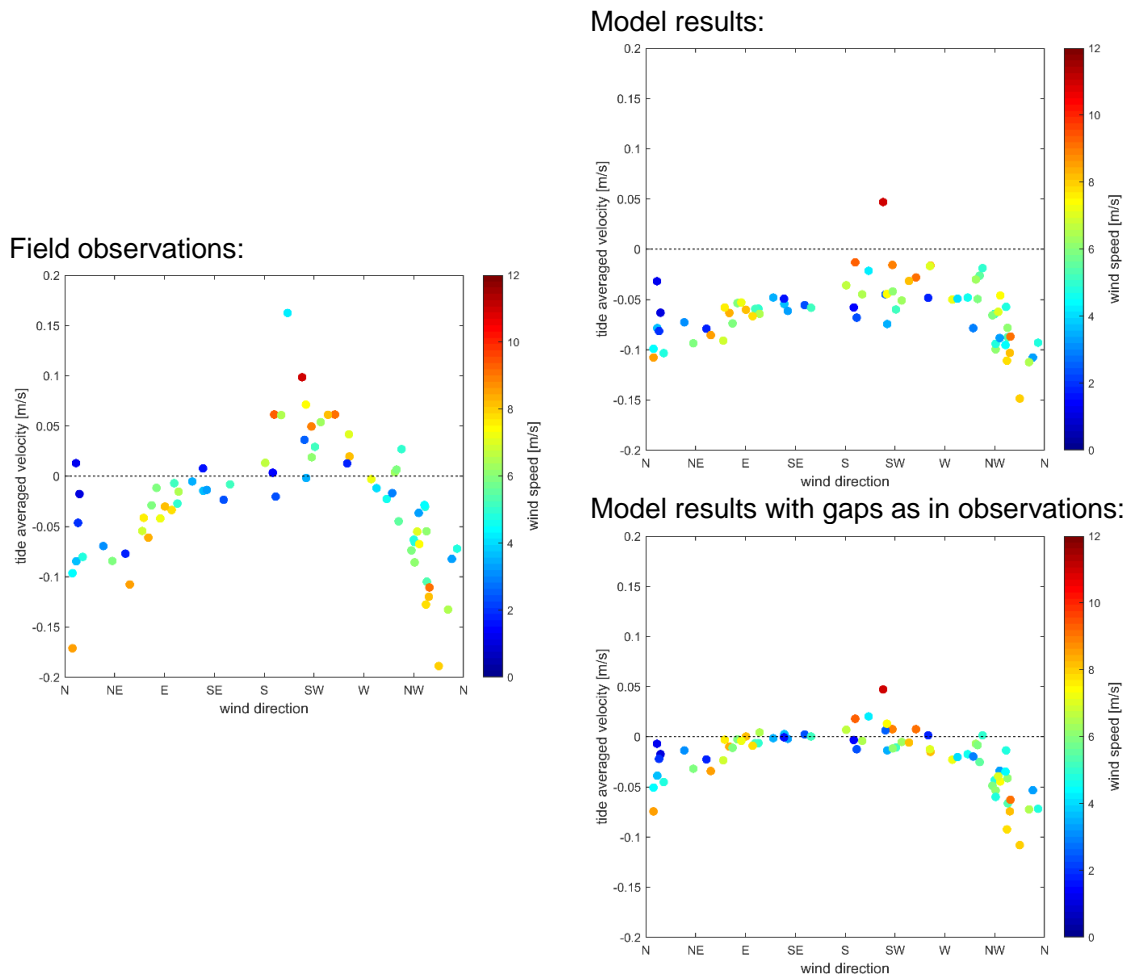

Figure 2.11 Tide averaged velocities depending on wind direction and wind strength, computed from observations (left) and model data (right). With the model data the tide averaged velocity is computed for the full tidal cycle (top right) and for the exact equal time steps that also observations are available (bottom right).

2.3 Waves

The current hydrodynamic Delft3D-FM model does not include waves. However, waves are important for resuspension of sediments, and subsequent transport by tidal currents. The effect of waves on sediment transport is parameterized using a fetch length approach. The input for this simplified wave model consists of time series of the wind speed and wind direction, the water depth and the fetch length, which varies per wind direction. The input values are used to compute the wave height, the wave length and the wave period, which are then used to compute the bed shear stress due to waves.

Time series of the wind speed and the wind direction as measured at KNMI station Hoorn Terschelling are used as model input for the wave computations (see Figure 2.12). The temporal resolution of this data (Δt) is 1 hour. The fetch lengths considered appropriate for the study site are listed in Table 2.1. The fetch length varies per wind direction bin of 45°. Note that the fetch length is spatially uniform, which is physically not correct, but sufficiently detailed for the purpose of this study.

Despite the simplified approach, the computed wave heights (see Figure 2.14) show good agreement with observations in the field (see Figure 2.13) at the Koehoal mudflat.
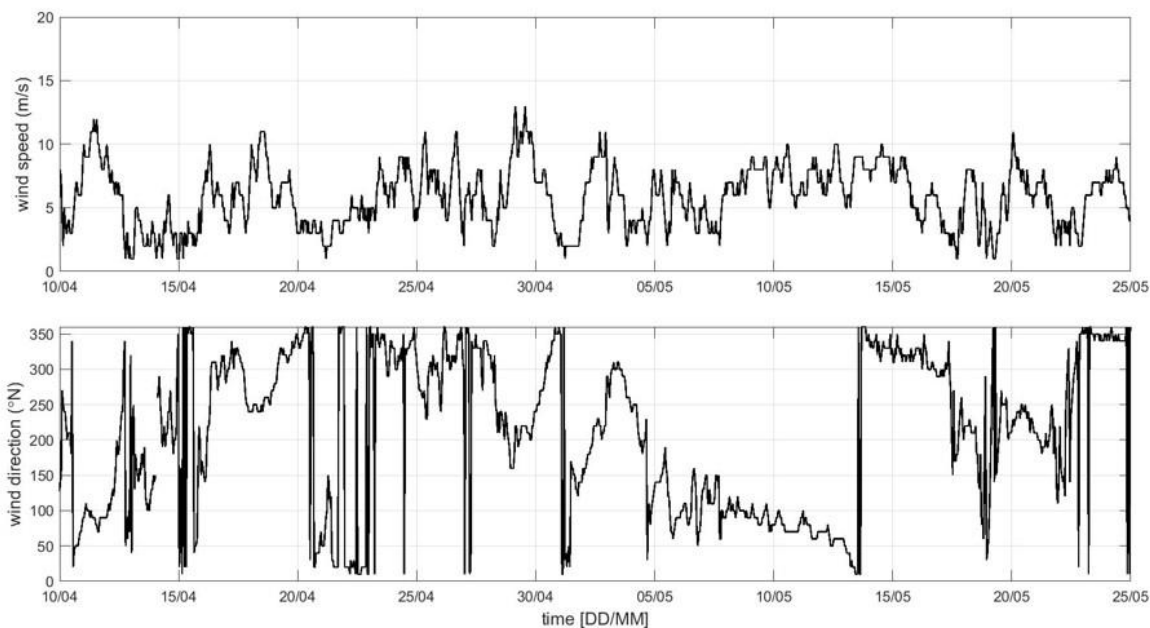

Figure 2.12 Timeseries of the wind speed (top) and wind direction as measured at KNMI station Hoorn Terschelling. These timeseries are used as input for wave computations.

Table 2.1   Fetch length per wind direction bin of 45°.

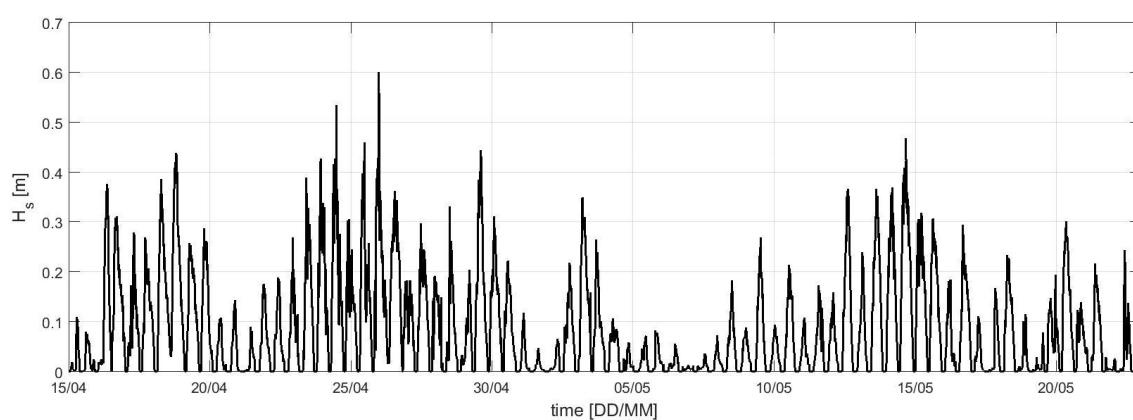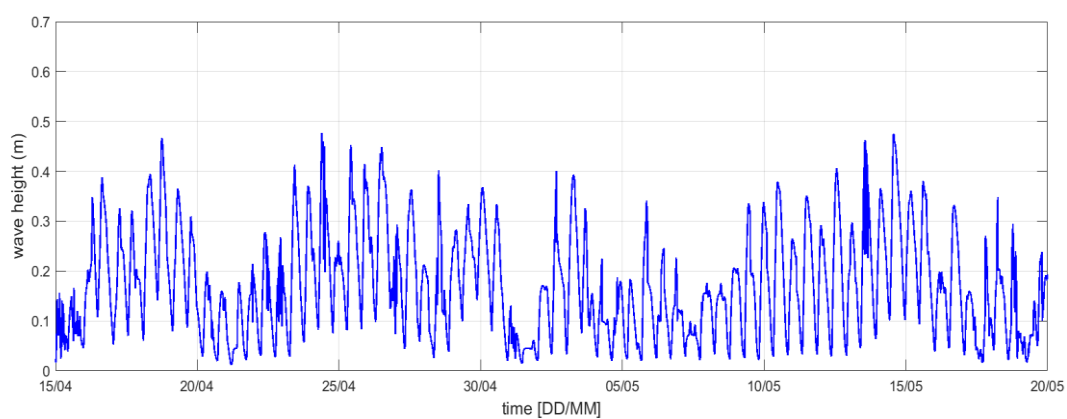| WIND DIRECTION (°N)	FETCH LENGTH (M)
0 – 45	15 000
45 – 90	5000
90 – 135	1000
135 – 180	1000
180 – 225	1000
225 – 270	20 000
270 – 315	15 000
315 - 360	10 000

Figure 2.13 Timeseries of the significant wave height H_s as observed during the field campaign near observation point Frame 1 (lower mudflat).

Figure 2.14 Wave heights at observation point Frame 1 (lower mudflat), as computed by WAQ based on the fetch length and measured timeseries of the wind speed and direction.

3 Fine sediment modelling

3.1 Model setup

The simulation time of the sediment transport model is from April 10th till May 25th, 2016. This period covers the field campaign on the Koehoal mudflat from April 14th till May 23rd. The sediment transport model is set up in the Delft3D-Water Quality module (WAQ).

The model bathymetry is not updated during the simulation and there is no influence of the sediment on the hydrodynamics (i.e. uncoupled sediment transport computation). The latter is only important for high sediment concentrations, much higher than occur in our study site. The communication from the hydrodynamic to the sediment transport model occurs every 30 minutes. The computation time step in WAQ is set to Δt = 1min.

The resolution of the hydrodynamic grid is aggregated 4x4 to reduce computational time in WAQ. This leads to a resolution of the sediment transport model of approximately 400 m x 400 m in the Wadden Sea. Near the study site, the grid cells are 2x2 aggregated, which implies a horizontal resolution of approximately 200 m x 200 m. The computational grid of the sediment transport model near the study site is shown in Figure 3.1. The vertical discretization is set to 10 σ-layers, whereas the hydrodynamic model has 20 layers. The number of segments in the WAQ model after aggregation is 372020.
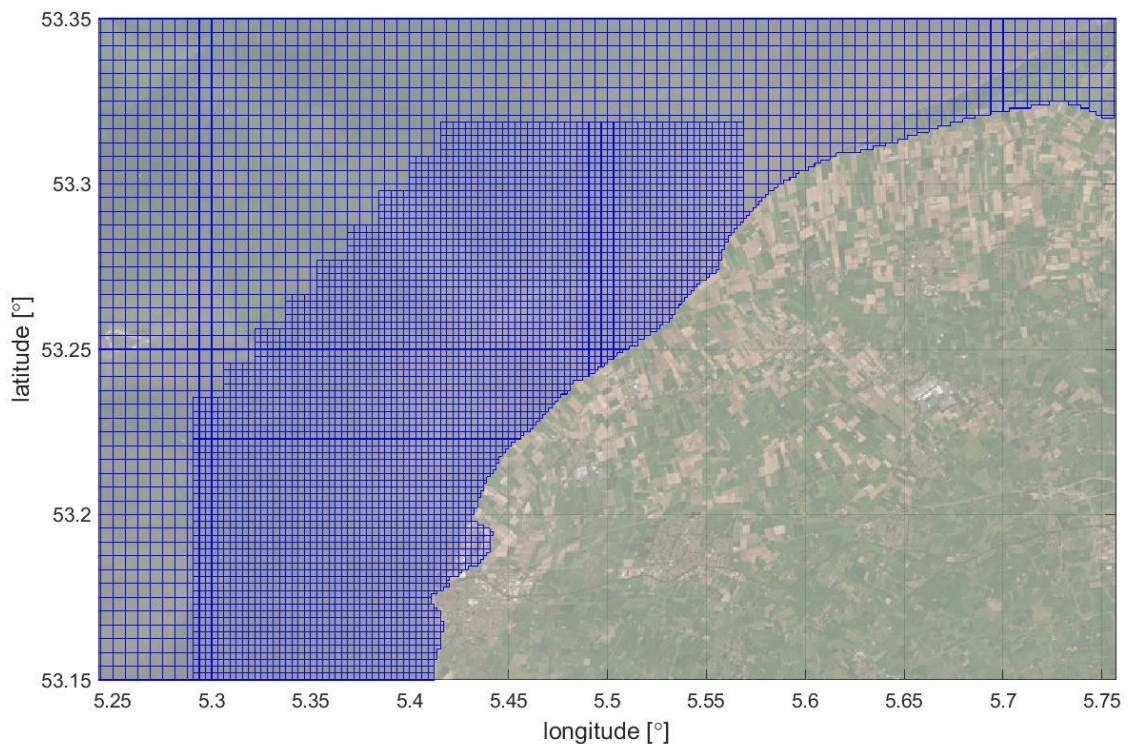

Figure 3.1   WAQ computational grid near the study site. Locally the hydrodynamic grid was 2x2 aggregated (i.e. new resolution approximately 200 m x 200 m), whereas in the remaining part of the model domain the hydrodynamic grid was 4x4 aggregated.

The sediment settings used in this study are copied from the earlier developed PACE model for mud dynamics in the Wadden Sea (van Kessel, 2015). These settings are listed in Table 3.1. Two different fractions of mud are included in the model simulations (i.e. IM1 and IM2), which differ in settling velocity. Fraction IM1 and IM2 can be considered as respectively macro and micro flocs. We also use a two-layer approach, which an easy to erode fluff layer on top of a more consolidated so-called buffer layer (see Van Kessel et al., 2011).

Table 3.1   Sediment parameter settings in the WAQ sediment transport model

PARAMETER	DESCRIPTION	VALUE
$w_{s,0}$ [mm/s]	settling velocity	IM1: 1.5 mm/s IM2: 0.20 mm/s
M_0 [kg/m^2/s]	erosion parameter	$1 \cdot 10^{-4}$
M_1 [1/s]	erosion parameter	$4.6 \cdot 10^{-7}$
M_2 [kg/m^2/s]	erosion parameter	$3.5 \cdot 10^{-7}$
$\tau_{1,cr}$ [Pa]	critical shear stress for resuspension fluff layer	0.1
$\tau_{Shields}$ [Pa]	Shields shear stress for resuspension buffer layer	1.0
α [-]	fraction sedimentation towards buffer layer	0.05
p_{dep} [-]	deposition efficiency	0.1
d_2 [m]	thickness of the buffer layer	0.1

The combined bed shear stress by currents and waves should be such that sediment transport is towards the tidal flat during low to moderate wave conditions, but the tidal flats is not completely eroded during high wave events. The contribution of currents and waves to the bed shear stress is calibrated by varying the Manning roughness coefficient for waves in Delwaq. In the sediment transport model, the bed shear stresses due to currents (τ_{flow}) are taken from the hydrodynamic model. A uniform Manning roughness of 0.020 s/m$^{1/3}$ is used in computing τ_{wave} at the study site. Eventually, the bed shear stresses due to flow and due to waves are summed to a total bed shear stress τ ($\tau = \tau_{wave} + \tau_{flow}$).

Figure 3.2 shows the total bed shear stress per grid cell on April 30th, when wave heights exceed 0.35 m at Frame 1 (see Figure 2.14). At this specific moment the bed shear stress at the shallow flats is up to 2.5 Pa. The bed shear stress due to currents only (see Figure 3.3), do not exceed 1.5 Pa, and are maximal in the channel. This clearly reveals the large contribution of waves in the total bed shear stress, especially at shallow areas.
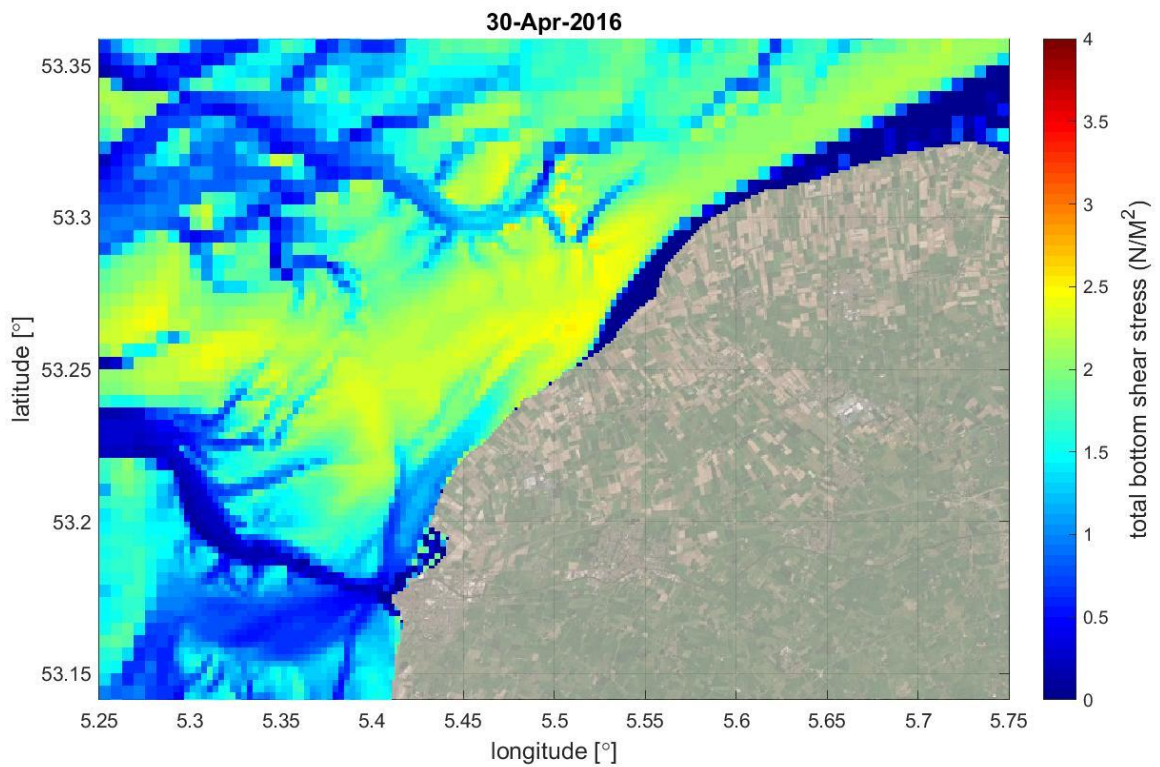
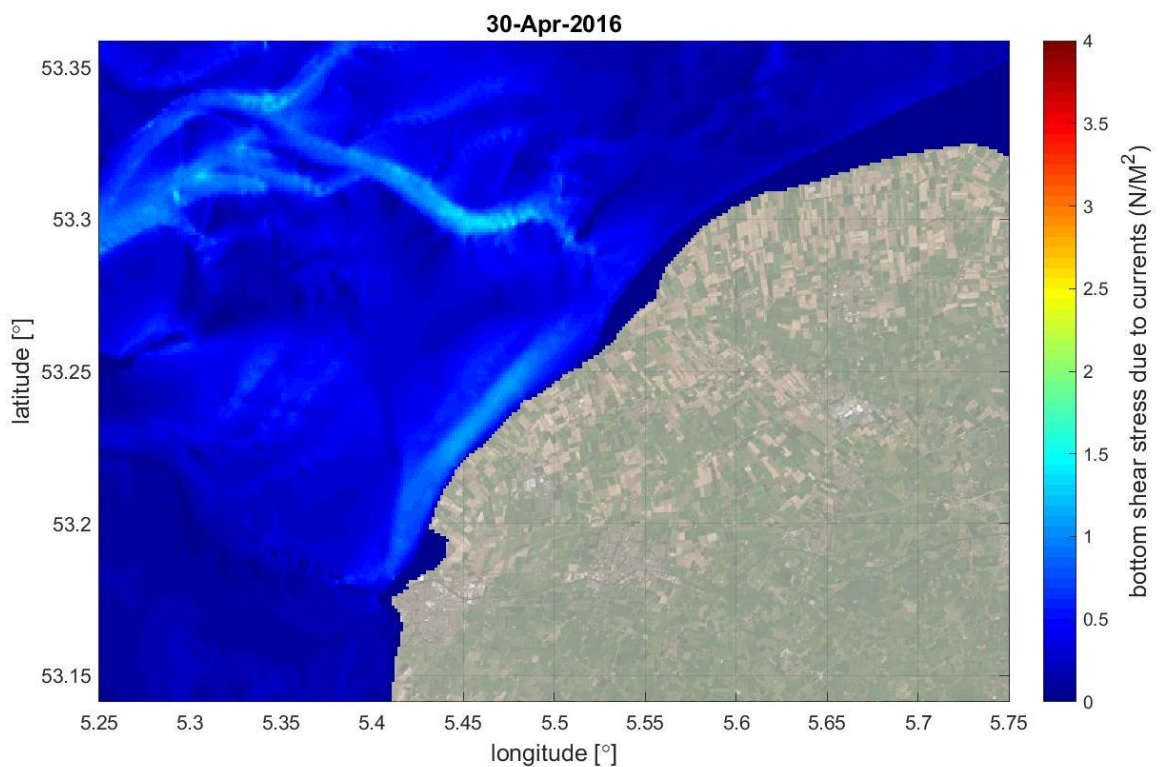*Figure 3.2   Total bed shear stress (by currents and waves) at April 30th, as computed by WAQ.*

Figure 3.3   Bed shear stress due to currents only at April 30th, as computed by the hydrodynamic Delft3D-FM model.

The Kimstergat channel is flood-dominant (Schulz & Gerkema, 2018), which is further illustrated by timeseries of the total bottom shear stress at an observation point in the Kimstergat channel in Figure 3.4. On top of this tidal signal, waves introduce an additional variability in the total bottom shear stress (most prominent at 18 April).
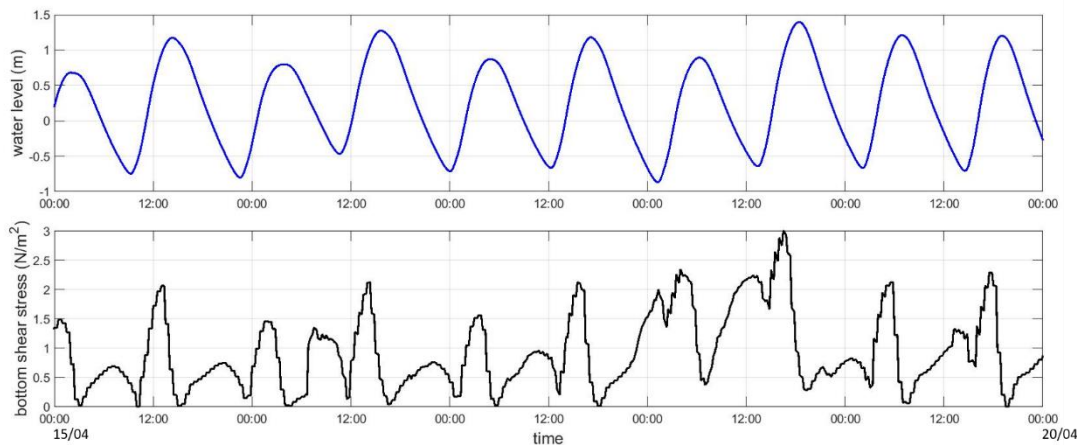

Figure 3.4   Timeseries of the computed water level at Harlingen (top) and the total bottom shear stress (by currents and waves) at an observation point in the Kimstergat channel (bottom).

3.2   Model approach

In the current version of the sediment transport model we focus on the mud motor disposal exclusively. This means that there is no sediment at the bed initially and no sediment will enter the model domain at its boundaries[1]. The only source of sediment is the mud motor disposal. This approach is followed for two reasons:

(1) The dispersal of sediment from the disposal location can be closely monitored, providing information on the fate and transport of mud motor sediments. The disposed sediment is not mixed up with sediment already available at the bed, and there is no need to label the disposal sediment in order to distinguish it from other sediments. This saves computational time.

(2) It avoids the setup of a background sediment concentration model, which is time-consuming.

The downside of the approach is that the sediment transport between the different morphological entities (tidal flats, tidal channels, coasts etc.) is influenced by the amount of sediment that is available at these locations and hence of the duration of the simulation. Sediment cannot be transported from an area where no sediment is available, and it takes time before the disposed sediments are dispersed within the study area. Therefore, 1) we use a spin-up time, although it is short (~8 month, constructed of 5 repeating hydrodynamic periods), 2) we dispose the sediment at the mud motor disposal location continuously, so more sediment becomes available in the model domain, 3) we restart with and without disposal to investigate redistribution of sediment after disposal and 4) we interpret the results taking the available amount of sediment into account.

---

[1] *A version of the model with a completely spin-up bed composition (amount of sand and mud in dynamic equilibrium) will be developed in related projects.*

By different model runs different aspects of the mud dynamics at the study site are investigated. The different model runs are introduced in Table 3.2 and explained in more detail below.

Table 3.2   Overview of the different model simulations that are discussed in this study

	SIMULATION NAME	INITIAL CONDITION	SEDIMENT DISPOSAL	PERIOD
1	Spin up	no (empty system)	continuous	5 x 45 days
2	Load	result of run 1	continuous	5 x 45 days
3	No load	result of run 1	no	5 x 45 days

The hydrodynamic simulation period from April 10th till May 25th, 2016 (45 days) is repeated five times to increase the simulation time of sediment transport computations. The sediment in the system (i.e. water column and bed) at the end of a hydrodynamic cycle of 45 days is then used as the initial condition for the next 45 days. Timeseries of the wind speed and the wind direction, and thus the wave conditions and bed shear stresses, are also repeated in every hydrodynamic cycle of 45 days. The total simulation period hence is 10x45 days, which is one year and 3 months. This is insufficient to reach dynamic equilibrium (especially for IM1), but sufficient to assess the impact of the Mud Motor.

At a selected set of model runs sediment is brought into the system by a continuous disposal of material. In this way the disposal of dredged material from a dredging vessel is simulated in a simplified way, because in reality sediment was only disposed during high water. The disposal location is in the northeastern part of the Kimstergat channel (5.44412° E 53.22164° N). The location is indicated by the white dot in Figure 3.5. At this location 50 kg/s per sediment fraction is disposed, adding up to a continuous disposal of 8640 ton per day. The total sediment mass released is 3.9 10^6 ton for simulation 1 + 2, and 1.9 10^6 ton for simulation 1 + 3.

There are five observation points included in the model, their locations are shown in Figure 3.5. Observation points *1: Frame 1 (lower mudflat)* and *2: Frame 2 (higher mudflat)* are at the locations of the measurement frames during the field campaign in spring 2016. The other three observation points are located in the Kimstergat channel. Also, 8 different observation areas are defined (Figure 3.6). For each of the observation areas the mass balance and the gross exchange with neighboring areas are available as output of the model simulation, which provides the opportunity to trace the distribution of sediment over areas.
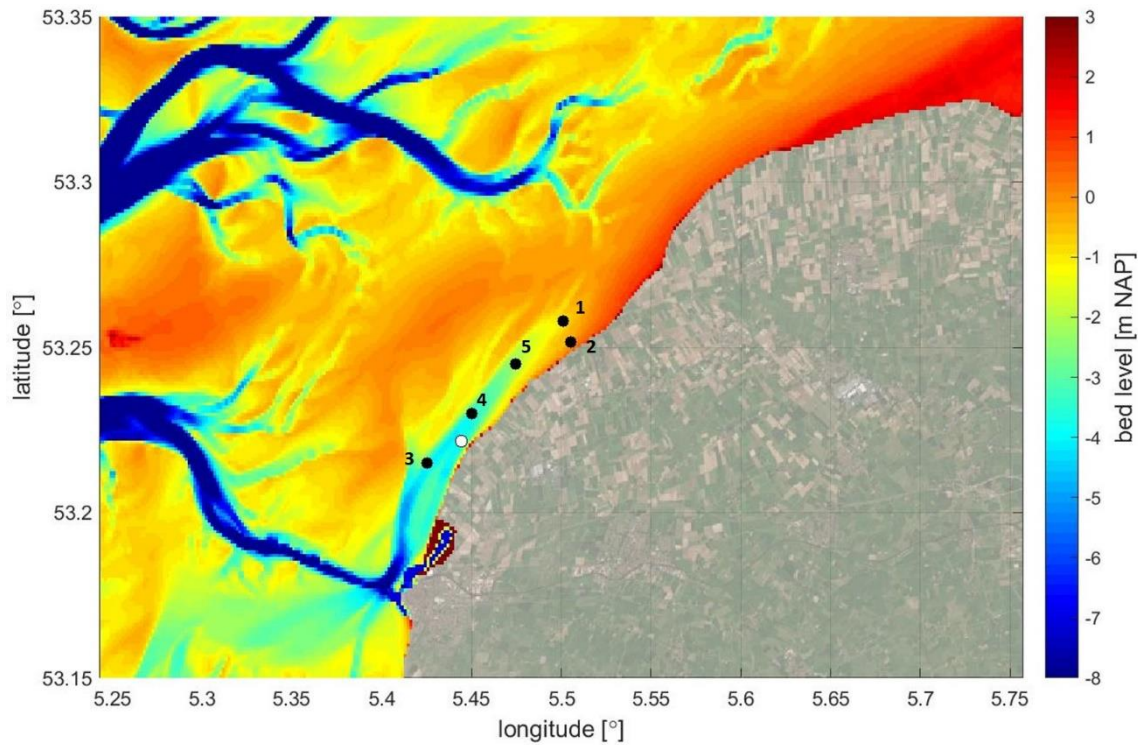
Figure 3.5   Bathymetry of the hydrodynamic model with indicated the disposal location (white dot) and the five observation points: 1: Frame 1 (lower mudflat), 2: Frame 2 (higher mudflat), 3: Kimstergat1, 4: Kimstergat2 and 5: Kimstergat3.
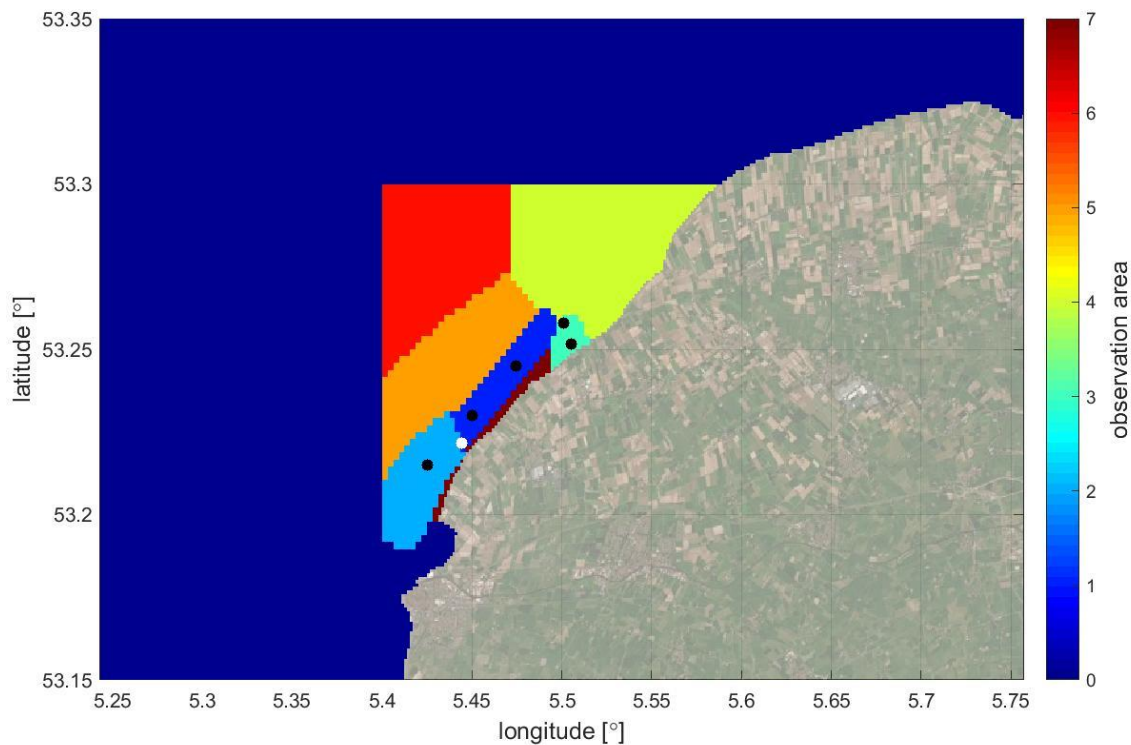

Figure 3.6   Location of observation areas, often referred to by the following names: 0: Far-field, 1: Kimstergat East, 2: Kimstergat West, 3: Flat_frames, 4: Flat_northeast, 5: Flat_northwest, 6: Flat_north and 7: Coastline.

3.3 Model results

3.3.1 Distribution of disposed material

The model simulation starting with an empty model domain and with a continuous disposal of sediment (spin-up) provides insight in where the disposed sediment is transported to and at what locations it deposits. The amount of sediment in the bed (both layers) after a simulation period of 5 x 45 days differs for IM1 (Figure 3.7) and IM2 (Figure 3.8). The coarse fraction (IM1) shows a clear sedimentation footprint that extends mostly northeast of the disposal location, whereas the finer fraction (IM2) is mainly transported south of the disposal location (i.e. near Harlingen) in a much thinner layer (i.e. lower quantities in the bed). A large amount of this fine material accumulates in the port of Harlingen. The difference in settling velocity between the two sediment fractions thus seems to have a large impact on the fate of the disposed sediment as well as the deposition rates.

Figure 3.7 and Figure 3.8 also show that much of the disposed sediment settles on the narrow intertidal area between Harlingen and Koehoal. The Kimstergat channel flows very close to the dike at this stretch and is only separated from the dike by short cross-shore groins (included in the hydrodynamic model, but not in the wave computations). Bed level observation data ('vaklodingen'), do not show this depositional behavior, but this may also be the result of limited coverage of these areas in the depth maps. The LiDAR surveys however, do reveal sedimentation in the most westward end of the study area near a groin (Baptist et al., 2019). This possibly suggests that the modelled sedimentation on this narrow fringe is realistic.
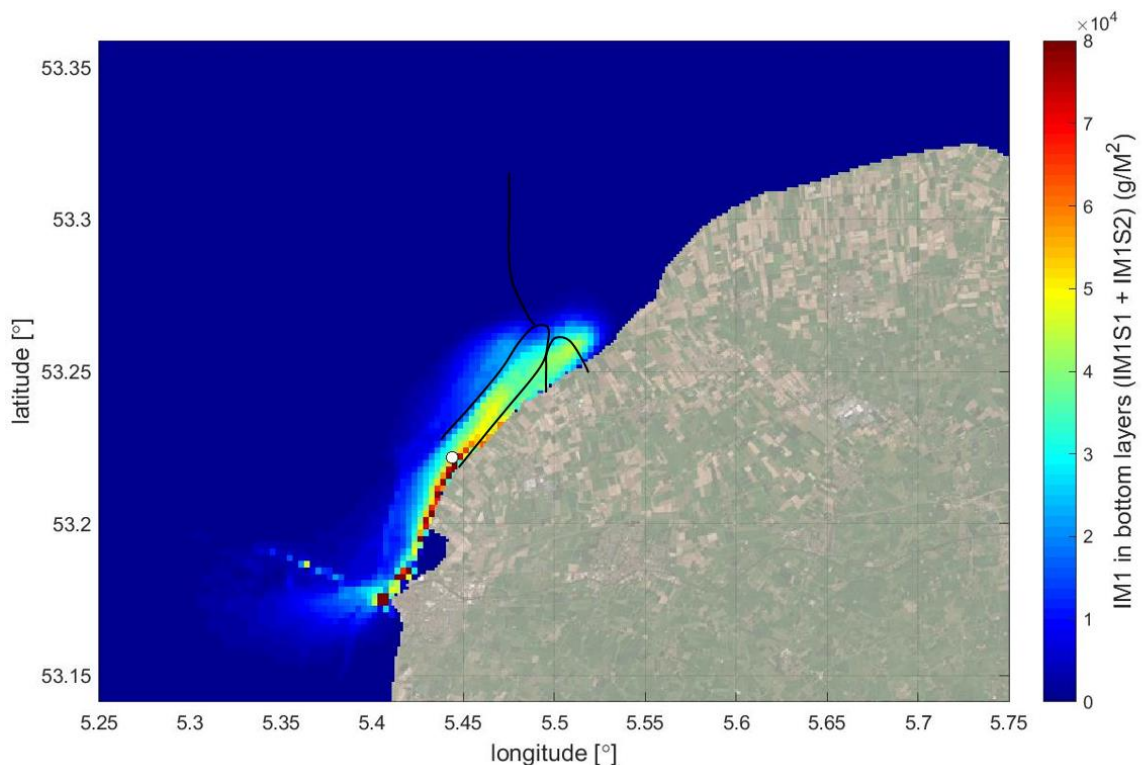

Figure 3.7   Coarse fraction (IM1) in the bed (sum of layer S1 and S2) after a simulation period of 5 x 45 days with continuous disposal at the disposal location (white dot). Black lines indicate the extent of the observation areas.
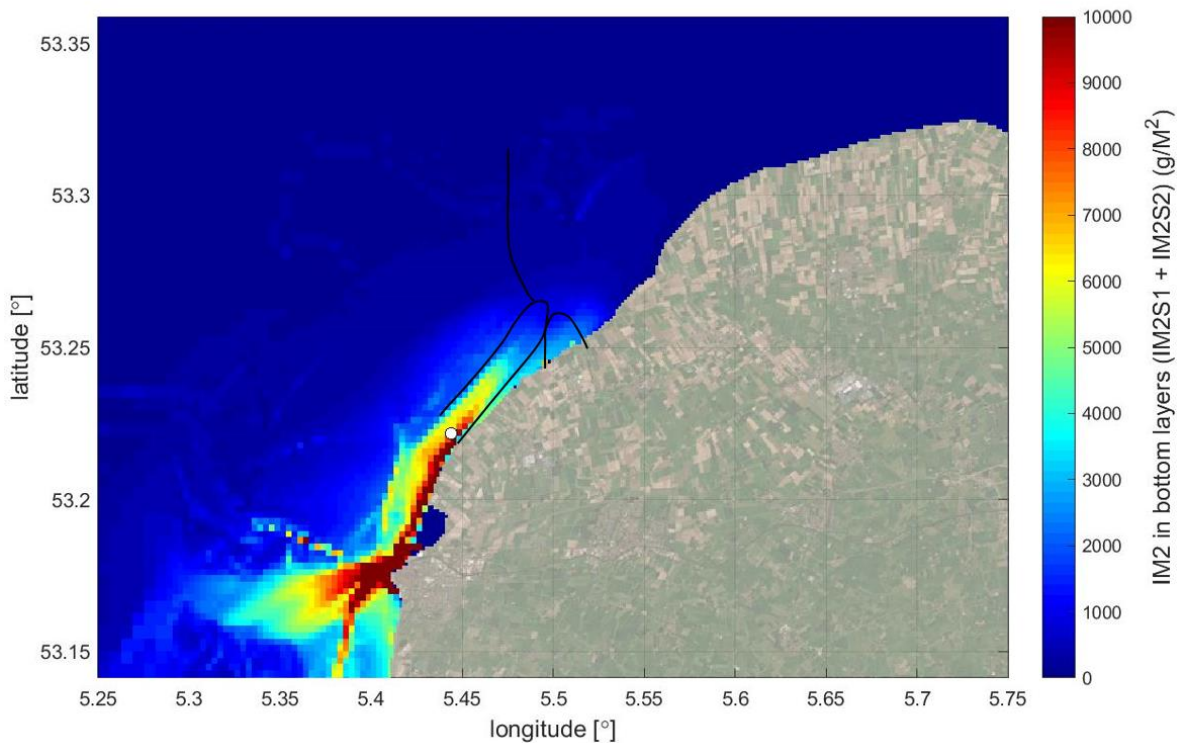
Figure 3.8   Fine fraction (IM2) in the bed (sum of layer S1 and S2) after a simulation period of 5 x 45 days with continuous disposal at the disposal location (white dot). Black lines indicate the extent of the observation areas.

The difference in behavior of the fine and coarse fraction can be explained with the residual flow. The residual flow during the study period is directed southward. North of the disposal location, this residual flow is large relative to the tidal flow (25%, see Figure 3.9). Sediments with a large settling velocity (IM1) are sensitive to lag effects introduced by a spatial gradient in flow velocities (high in the channel, low on the flat) in combination with a critical shear stress for erosion. Sediments in the channel are eroded at the start of the flood, subsequently transported landward, and settling around high water. During the following ebb, they are eroded in a later phase of the tidal cycle because the flow velocities are lower on the flat. They are therefore transported seaward for a shorter distance than the landward transport during the flood. This effect is much more pronounced for sediments with a large settling velocity (IM1) than sediments with a low settling velocity (IM2), because the latter sediment hardly settles during high water slack. This effect is even enlarged by the deposition efficiency, which is set to 0.1, implying that only 10% of the sediment that may reach the bed during a timestep, is depositing at the bed. This value for the deposition efficiency is chosen based on modelling experience with the PACE model and other numerical models for similar systems. It compensates for the lack of vertical resolution, underestimation of the hindered settling and the too high strength that the bed gains instantly upon settling, even when it is in the fluff layer. Because of the low exchange with the bed, the IM2 fraction is more susceptible to residual flows, leading to southward transport. Because of the relatively low settling velocity of IM2, particles remain in suspension until sedimentation occurs at low-energetic areas. Such areas are especially located in and southwest of the harbor of Harlingen (see e.g. Figure 3.2), hence the sedimentation of IM2 in this area is relatively high (see Figure 3.8).

Model simulations with and without additional sediment disposal (number 2 and 3 in Table 3.2, which use the results of model simulation 1 as initial conditions), are used to examine the exchange of sediment between different areas and the effect of the sediment disposal on these exchanges. In general, continuing the disposal (Figure 3.10 and Figure 3.12 for IM1 and IM2 respectively) leads to a continuation of the depositional behavior as observed in Figure 3.7 and Figure 3.8. After the disposal of sediment has stopped, sediment still spreads over the area (Figure 3.11 and Figure 3.13 for IM1 and IM2 respectively). This still causes a residual transport of both fractions from the Kimstergat to the intertidal areas. The difference again is that IM2 is mostly transported to the south, whereas IM1 is also still transported north of the disposal location. At some distinct locations the sediment IM1 in the bed has increased during simulation 3. The Koehoal mudflat is one of these locations (Figure 3.11). This is in line with the results of our tracer experiment, in which the amount of tracer particles at the Koehoal mudflat was increasing over the course of a month.
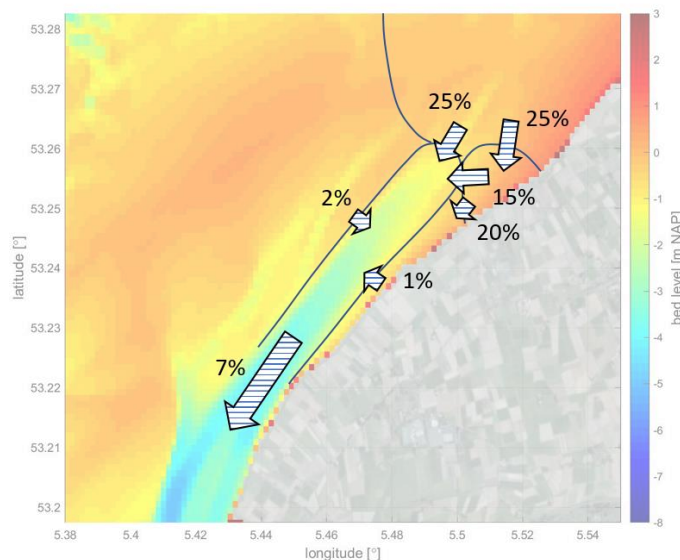

Figure 3.9   Illustration of the residual discharges between different areas, averaged over a period of 45 days. The size of the arrows indicates the relative size of the discharge. The percentage the magnitude of the residual discharge relative to the gross discharge.

After 10×45 days of continuous disposal (see Figure 3.10), the total mass of sediment at the Koehoal mudflat (Flat_frames) is approximately 120 000 tons IM1 and 5 000 tons IM2, equivalent with ~80 kg/m^2. The total sediment disposal over this period is 3.9 10^6 tons per fraction. This would imply 6% of IM1 has been transported to the Koehoal mudflat and 0.25% of the disposed IM2, or 3% of the total disposal. Here it is again mentioned that the disposal in this modelling study is done continuously, whereas in the Mud Motor pilot the sediment was only disposed at high water. Assuming the flow is in flood direction for about half the time, and none of the sediment disposed during ebb deposits on the Koehoal flat, would imply approximately 12% of the disposed IM1 during flood is found at the Koehoal mudflat after 10×45 days, or 6% of the total disposal. If the ~10% efficiency is translated to a sediment thickness for the Mud Motor pilot with a disposed volume of 470,000 m^3 in the hopper, this is equivalent to ~3 cm of unconsolidated material, or ~1.5 cm more consolidated material. This is smaller than the vertical accuracy of the LiDAR surveys, and smaller than the natural bed elevation

dynamics in the area. And this is the same sedimentation thickness that was derived from the tracer experiment in the major part of the study area (Vroom et al., 2017).[2]

The qualitative residual sediment transports between areas are indicated with arrows in Figure 3.14, both for the simulation with disposal in the Kimstergat channel (left) and without disposal (right). The timeseries of the model outcomes are included for reference in Appendix 1. The percentages in Figure 3.14 give a more quantitative insight in where the disposed sediment is transported to. The continuous disposal (i.e. also during ebb flow) results in a large residual transport of disposed sediment towards Harlingen, whereas the Mud Motor pilot disposal only took place at high water levels and hence during flood directed flow. Approximately 90% of the fine fraction is transported to the south, which partly explains why the fine sediment fraction is hardly found north of the disposal location (see Figure 3.8).
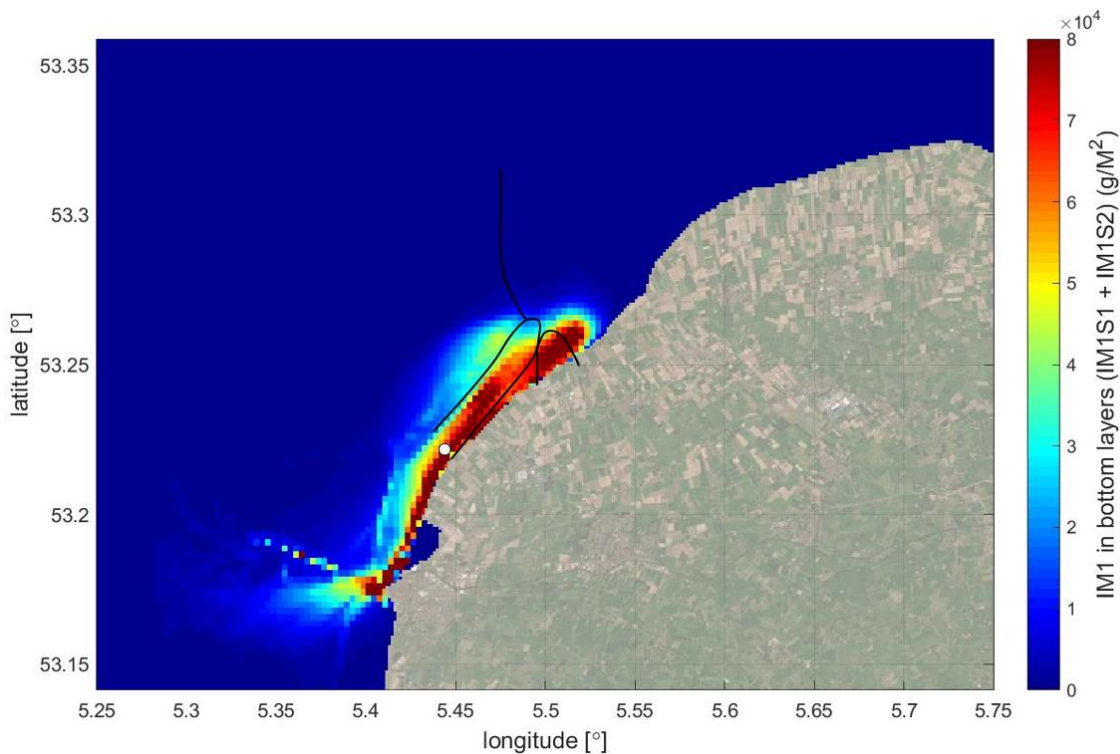

Figure 3.10 Coarse fraction (IM1) in the bed (both layers) after a simulation period of 10 x 45 days with continuous disposal (i.e. after simulation 2). Black lines indicate the extent of the observation areas.

---

[2] *In the tracer experiment we found that (after extrapolating) 80% of the disposed material was deposited at the study area, however, this area was much larger (~20km² vs. 1.5km² in this model study.*
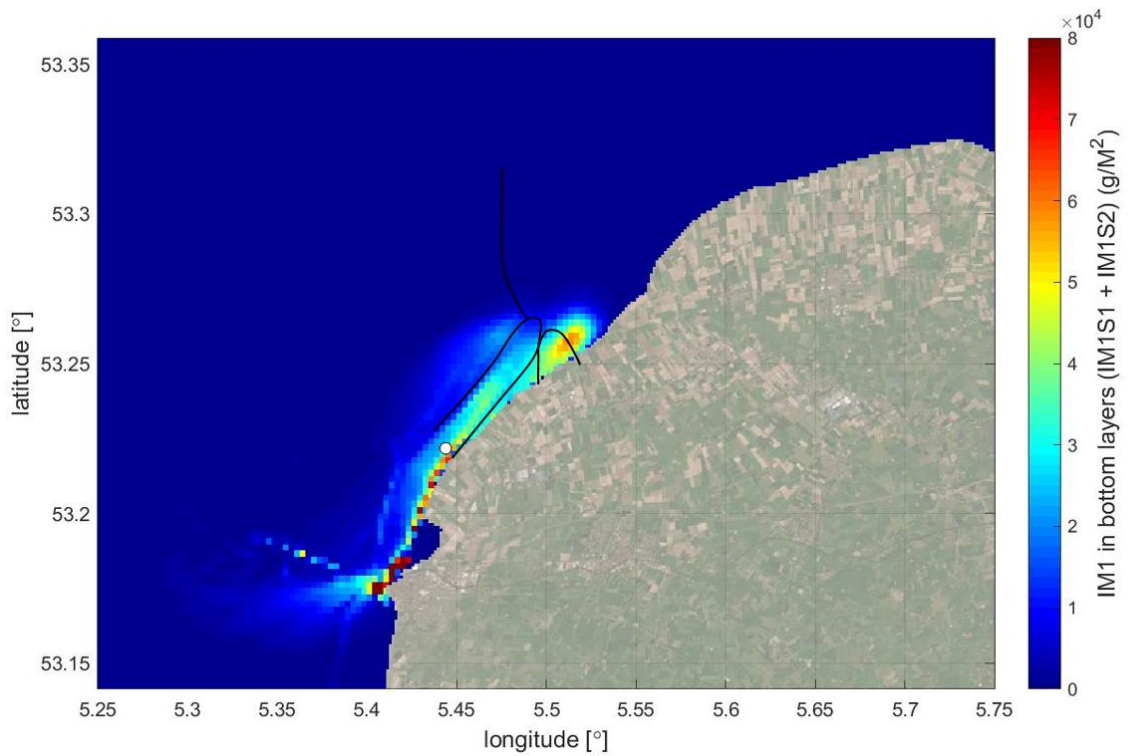
Figure 3.11 Coarse fraction (IM1) in the bed (both layers) after a simulation period of 5 x 45 days with continuous disposal and subsequently 5 x 45 days without disposal (i.e. after simulation 3). Black lines indicate the extent of the observation areas.
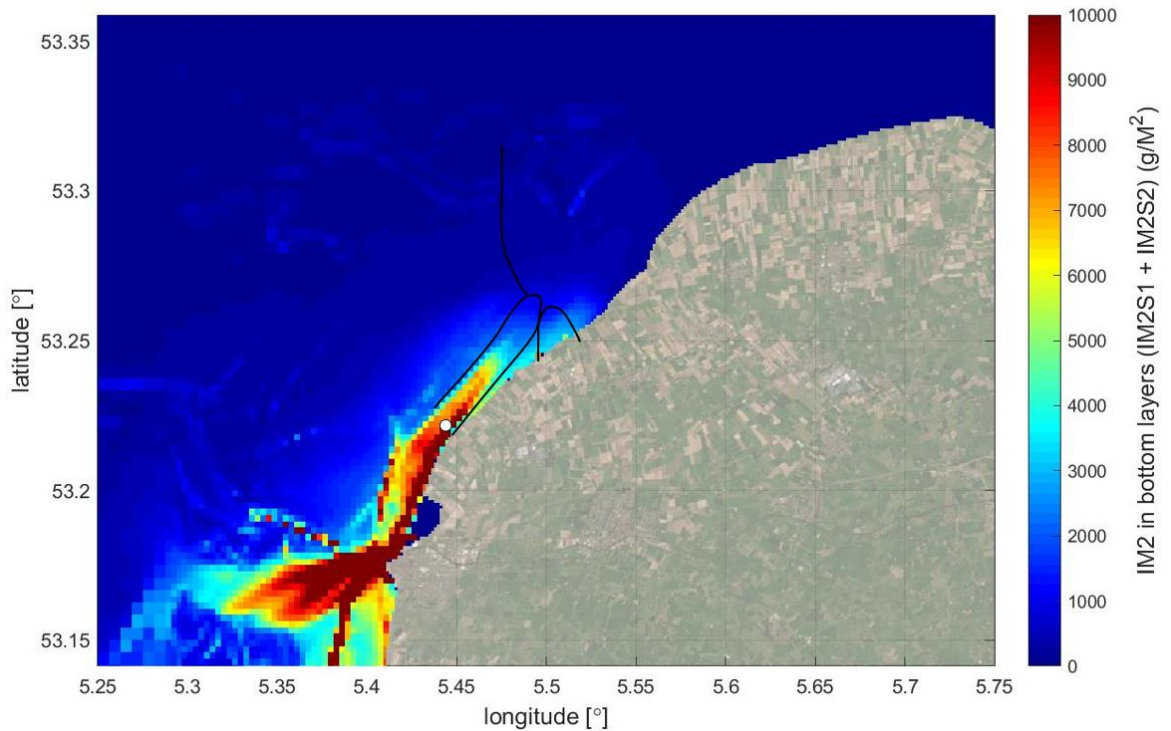

Figure 3.12 Fine fraction (IM2) in the bed (both layers) after a simulation period of 10 x 45 days with continuous disposal (i.e. after simulation 2). Black lines indicate the extent of the observation areas.
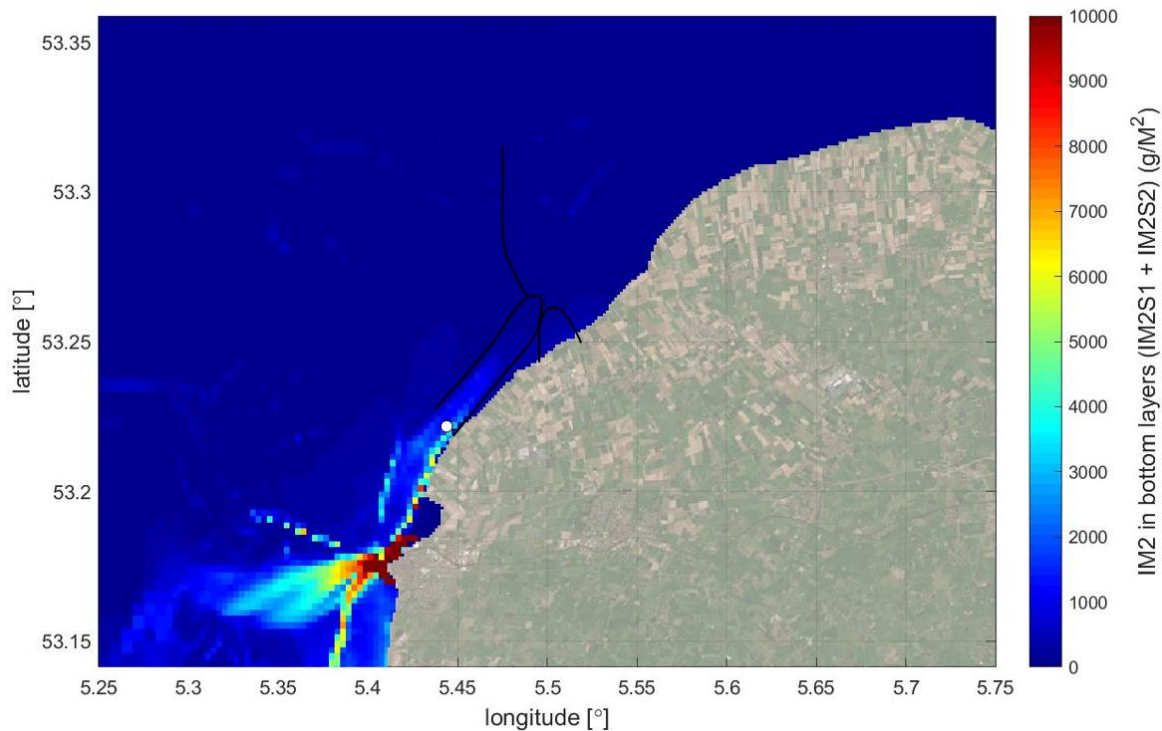
Figure 3.13 Fine fraction (IM2) in the bed (both layers) after a simulation period of 5 x 45 days with continuous disposal and subsequently 5 x 45 days without disposal (i.e. after simulation 3). Black lines indicate the extent of the observation areas.
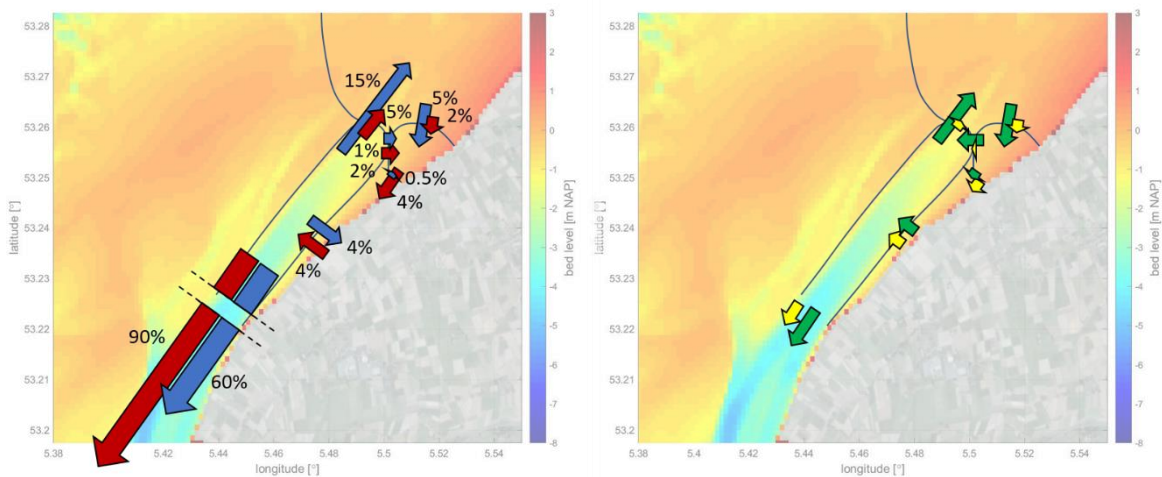

Figure 3.14 Illustration of the residual sediment transport between different areas in model simulation 2 (left, continuous disposal) and 3 (right, no disposal). The coarse sediment fraction (IM1) is illustrated in blue/green, the finer sediment fraction (IM2) is illustrated in red/yellow. The size of the arrows indicates the size of the flux, although the arrows towards Harlingen in the left figure are shortened. The percentages show the magnitude of the residual flux as a percentage of the disposal, averaged over the simulation time.

With a continuous disposal of sediment in the Kimstergat channel, residual transports of both sediment fractions are generally directed from the channel towards the different intertidal areas. An exception is the residual transport of IM2 between the Kimstergat channel and the coastal

stretch, which is directed towards the channel. A possible explanation is that residual discharges are directed from the shallow areas towards the deeper channel (see Figure 3.9) and that during the spin-up an equilibrium in IM2 bed sediment has been achieved in the coastal stretch. This is supported by Figure 3.15, which shows a dynamic equilibrium in the amount of IM2 sediment in the fluff layer during the simulations with disposal (i.e. 1 and 2). Similar behavior seems to be occurring between the frames area and the coastal stretch (directed southward for IM2). Hence, for the finer fraction IM2, there seems to be a recirculation cell from the Kimstergat, following the channel axis to the northeast and then deflecting to the coast and returning to the southwest near the coast.
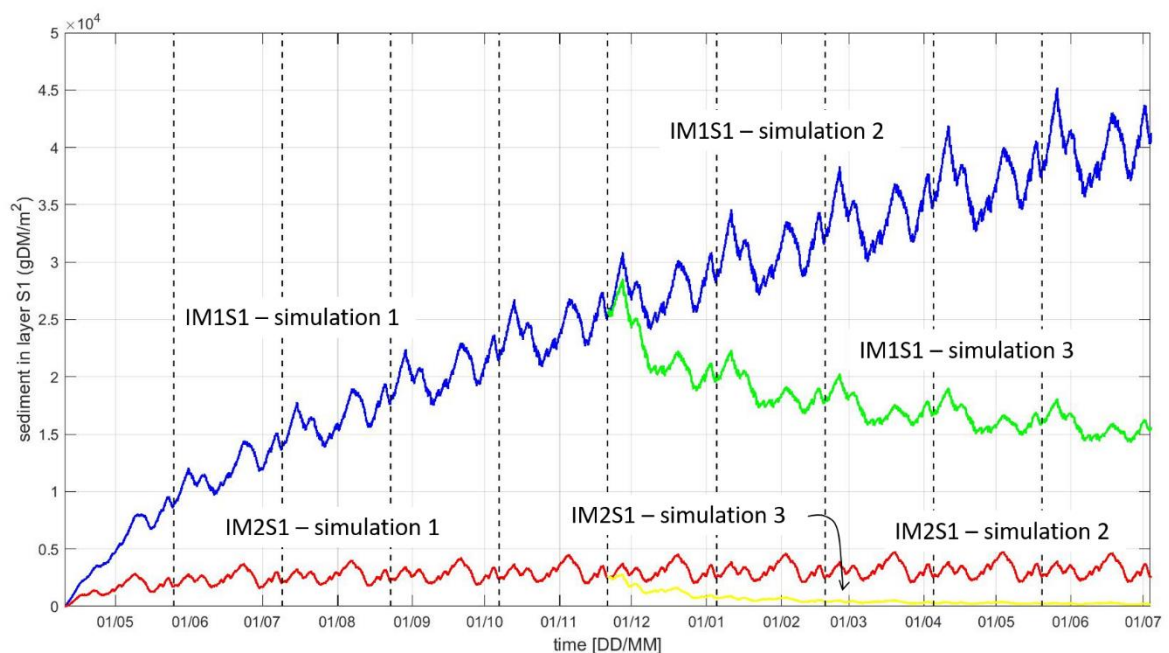

Figure 3.15: Sediment quantities in the fluff layer (S1) in the coastal stretch south of the Kimstergat (7: Coastline (see Figure 3.6)). Vertical dashed lines indicate blocks in which the hydrodynamic forcing is repeated. The first five blocks belong to the spin-up period (simulation 1). The second five blocks belong to either simulation 2 (continuing disposal) or simulation 3 (no disposal).

There is a residual transport from the northern flat area towards the Koehoal mudflat that is independent from the load, i.e. the sediment transport with and without load is in the same direction and the same order of magnitude. The southwestern corner of the 'northern flat area' shows a significant amount of sediment (mainly IM1) in the bed layers, resulting in resuspension and hence significant transport from the flats in the north towards the Koehoal mudflat. The presence of the load does increase the residual transport of the finer fraction though, most likely because the concentrations in the water column at location Frame 1 are higher in case the disposal continues (see Figure 3.16) and quickly reduces if the disposal is stopped. For the coarser fraction, the suspended sediment concentrations respond much slower to the absence of disposal. This is caused by resuspension of this fraction from the bed and larger availability of this fraction in the bed compared to IM2 (critical shear stress for erosion is identical for both fractions).
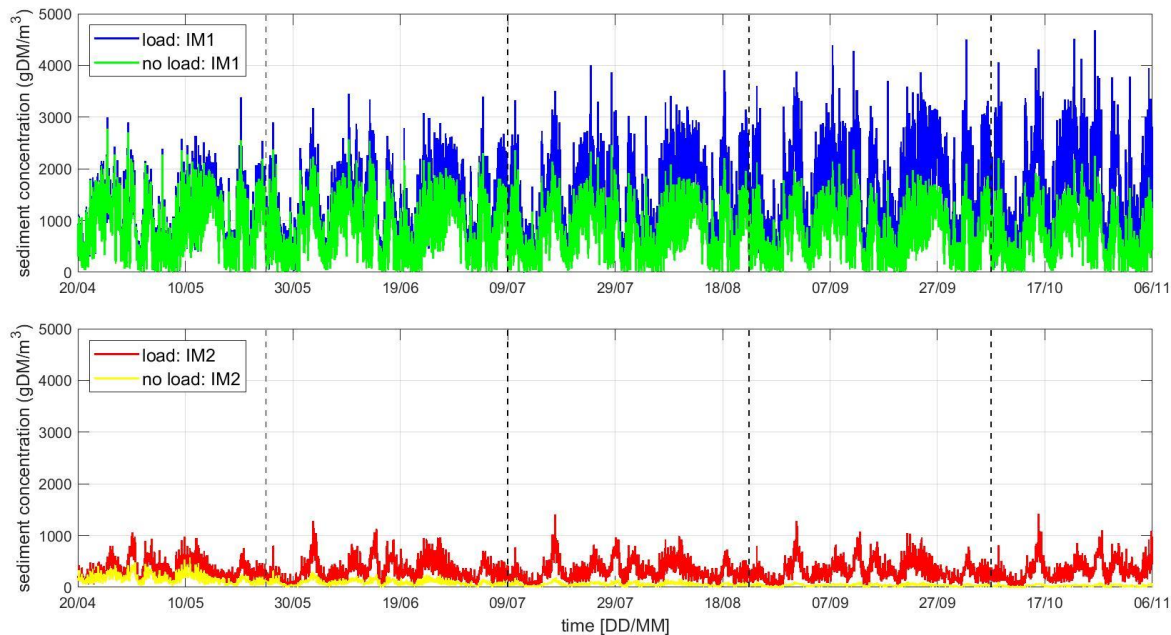
Figure 3.16 Timeseries of the sediment concentrations in the bottom layer of the water column at observation point 1: Frame 1 (lower mudflat) for IM1 (top) and IM2 (bottom) in model simulations with (blue/red) and without (green/yellow) continuing the disposal of sediment.

3.3.2 Residual currents and wind effects

In the previous section the cumulative residual sediment transports were discussed integrated over the entire simulation period. These can partly be explained by the magnitude and the direction of the residual discharge between different observation areas (see Figure 3.9). Because the finer fraction has relatively little interaction with the bed (i.e. particles are often in suspension), many of the residual sediment transports of the finer fraction can be explained by the residual discharges in combination with concentration gradients. Although we look at simulations after spin-up, the results are still affected by the divergent transport from the release location.

In the timeseries of the residual sediment transport, there is a clear variability in the direction and magnitude of the residual sediment transport over time at many of the cross-sections. Part of this variability can be explained by the wind forcing during certain periods (see Figure 2.12). To illustrate this the sediment exchange between the Kimstergat and the Koehoal mudflat is discussed (see Figure 3.17). Generally, the residual sediment transport is directed from the Kimstergat to the mudflat as a result of transport from high concentration to low concentration areas due to the disposal and due to the flood-dominant tidal flow in the Kimstergat channel (Figure 3.4). During certain events (e.g. at April 24th, April 26th, May 12th-15th and May 23rd-24th) the residual transports are in opposite direction. These events coincide with relatively strong winds (windspeed > +/- 8 m/s) from the north (approximately between -45°N and 45°N).
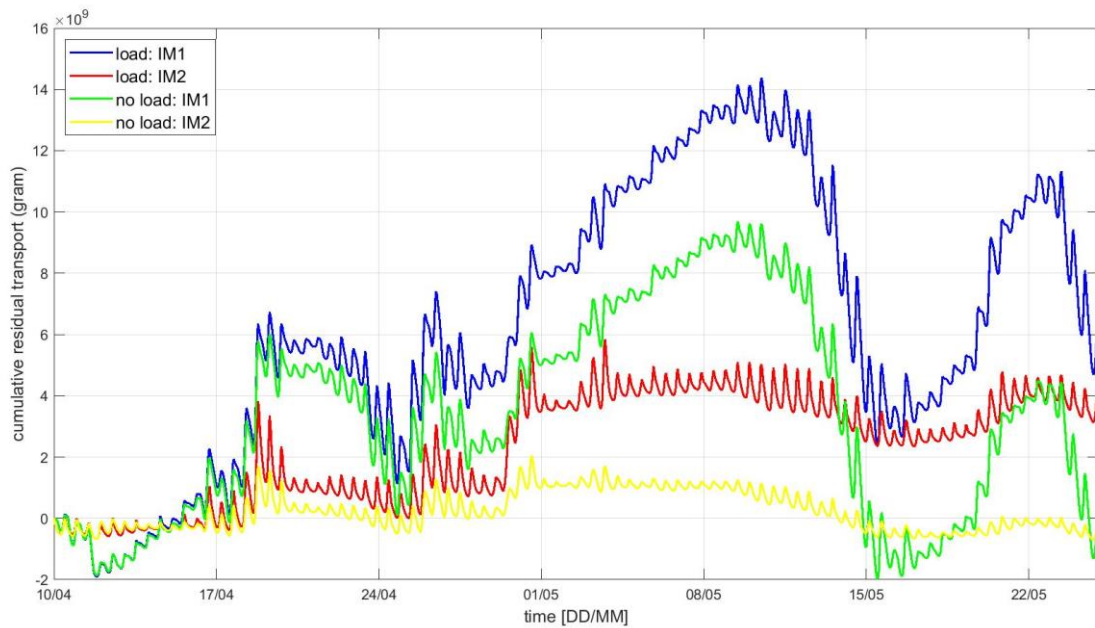
Figure 3.17 Timeseries of the residual sediment transport from the Kimstergat to the Koehoal mudflat (3: Flat_frames, see Figure 3.6) in the 45 days after spin-up.

So apparently, the direction of residual sediment transport is strongly determined by the wind forcing. The variability is investigated further by considering the residual sediment transport per tidal period, similarly as in Section 2.2 for the hydrodynamic results.

The residual sediment transports per tidal period between the Kimstergat and the northern flat (Figure 3.18), between the Kimstergat and the Koehoal mudflat (Figure 3.19) and between the Koehoal mudflat and the northern mudflat (Figure 3.20) are determined for the first 45 days of simulation 2. Using the results of simulation 3 (no disposal) would especially affect the results presented for IM2, since concentrations of IM2 would decrease if the sediment disposal is stopped. Concentrations of IM1 are less affected in the first 45 days after stopping the disposal (see Figure 3.16).
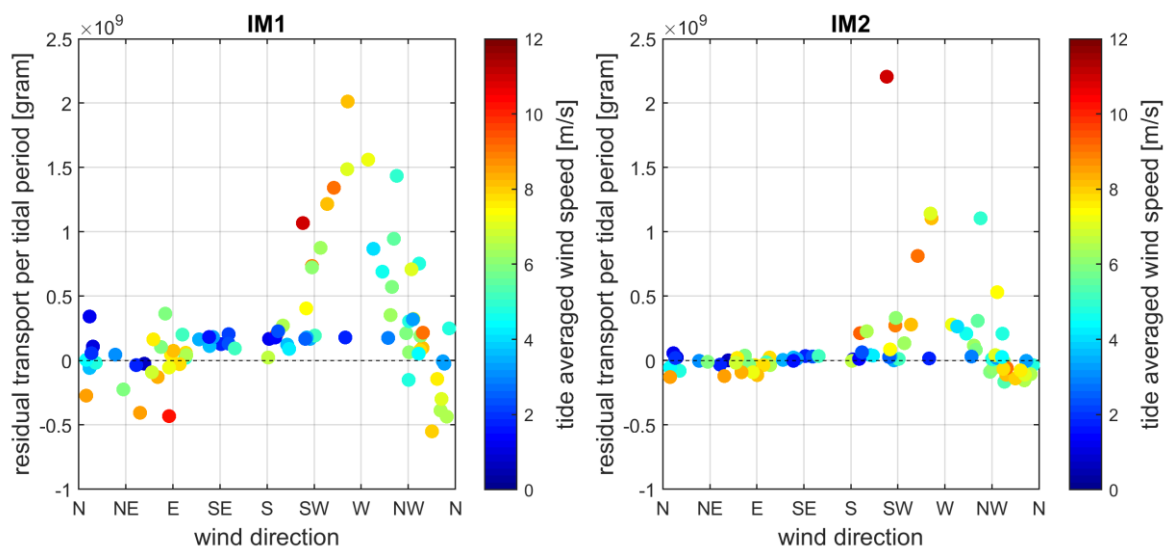

Figure 3.18 Tide averaged residual sediment transport of IM1 (left) and IM2 (right) from the Kimstergat (1: Kimstergat East) to the northern flat area (6: Flat_north) in relation to the tide averaged wind forcing.
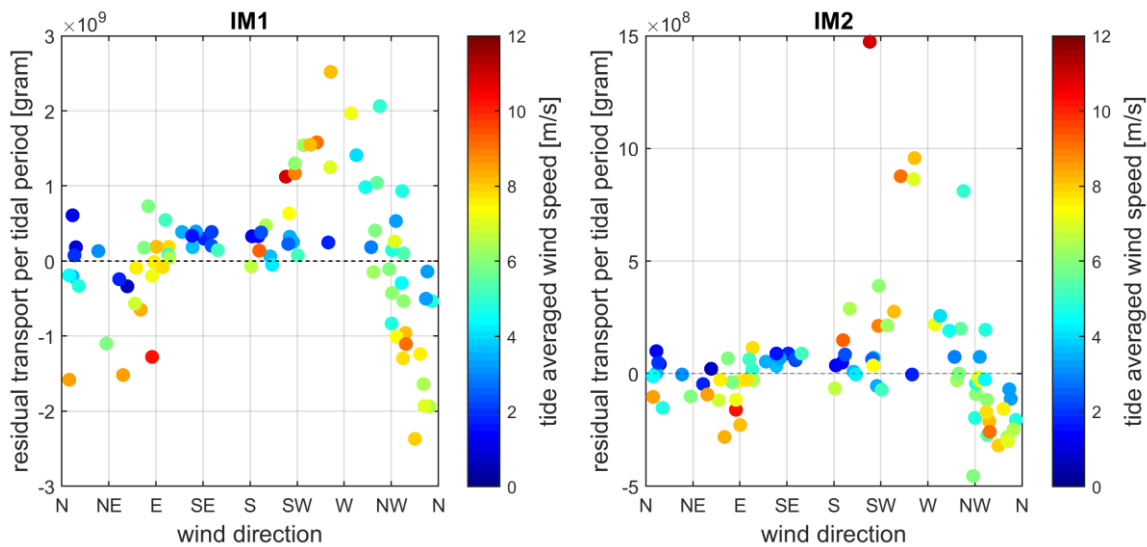
Figure 3.19 Tide averaged residual sediment transport of IM1 (left) and IM2 (right) from the Kimstergat (1: Kimstergat East) to the Koehoal mudflat (3: Flat_frames) in relation to the tide averaged wind forcing.
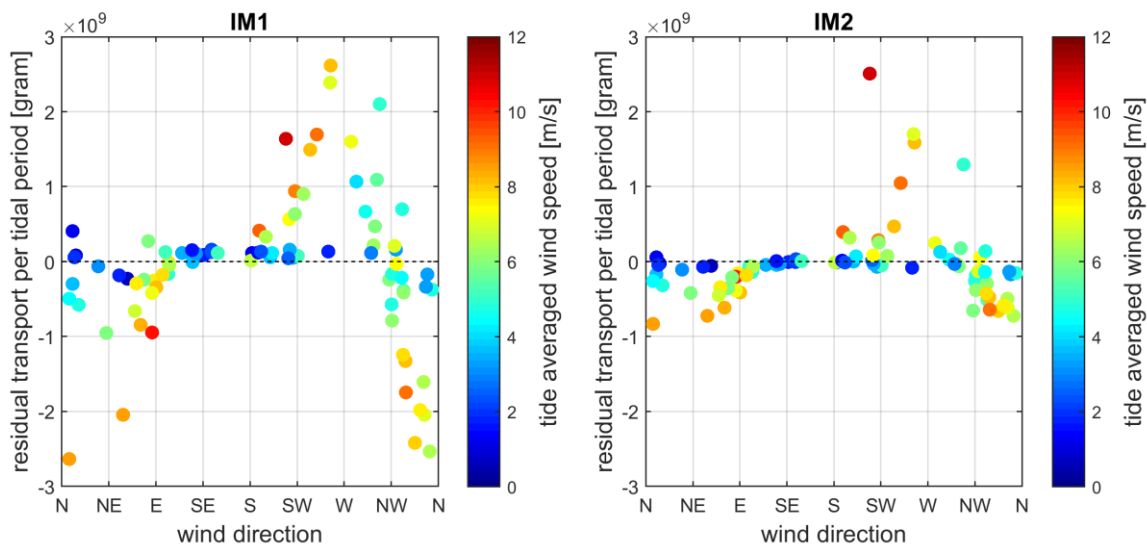

Figure 3.20 Tide averaged residual sediment transport of IM1 (left) and IM2 (right) from the Koehoal mudflat (3: Flat_frames) to the northern flat area (6: Flat_north) in relation to the tide averaged wind forcing.

The figures show that during low wind speeds, the residual sediment transport is low. During intermediate to strong wind, the sediment transport quickly increases. The coarser fraction seems to be more sensitive to wind than the finer fraction, although this is at least partly caused by the limited availability of IM2 on the intertidal flats. Wind forcing affects the residual sediment transport of IM1 by amplifying the current speed on the one hand and by generating waves and thus higher bed shear stresses on the other hand. Residual discharges, also influenced by wind (Figure 2.11), are an important mechanism for the transport of IM2.

During winds from the SW, sediment is transported out of the Kimstergat towards the northern flats (Figure 3.18), and towards the Koehoal mudflat (Figure 3.19). Also, sediment from the Koehoal mudflat is simultaneously transported towards the northern mudflat (Figure 3.20). These latter two transports are approximately equal in magnitude. Still, sedimentation does

take place at the Koehoal mudflat during SW wind (Figure 3.21). This can be explained by the amount of sediment transported from the coastal stretch towards the Koehoal mudflat. For example, on May 20th and 21st a relatively strong wind is coming from the southwest. The residual transport of IM1 from the Kimstergat to the Koehoal mudflat and from Koehoal mudflat to the northern flats are both around 5000 tons during this period. Also, around 4000 tons IM1 are transported from the coastal stretch to the Koehoal mudflat. Since the surface area of the Koehoal mudflat area is around 1.5×10^8 m^2, this leads to an increase of IM1 in the bed with approximately 3 kg/m^2 between May 20th and 22nd (as also shown in Figure 3.21). This means that cross-shore transport might be limited during (strong) SW wind.

During northern winds, sediment is transported in opposite direction and magnitudes are similar to SW wind transport (see also equally sized arrows in Figure 3.14). Only the transport from the northern mudflat to the Kimstergat channel is lower during northern winds than during SW wind, but this caused by the low availability of sediment in the northern flat area. The observation that sediment transports are equal in size during N and SW wind is hence also skewed by the sediment availability. If the tidal flats northeast of the frames area would be covered by an abundance of fine sediment (such as in reality), the transports from the northeast ("Terschellinger Wad") to the southwest would be much larger during NE winds (as also measured, see Colosimo et al. (in review). The underestimation of this flux from the NE on the modelled time scales suggests that (1) sediment that is transported from the NE towards the Koehoal tidal flats, does not originate from the Kimstergat but from elsewhere (i.e. Ameland tidal inlet, other parts of Vlie basin that are temporarily stored at the Terschellinger Wad) or (2) that the recirculation patterns is very local.
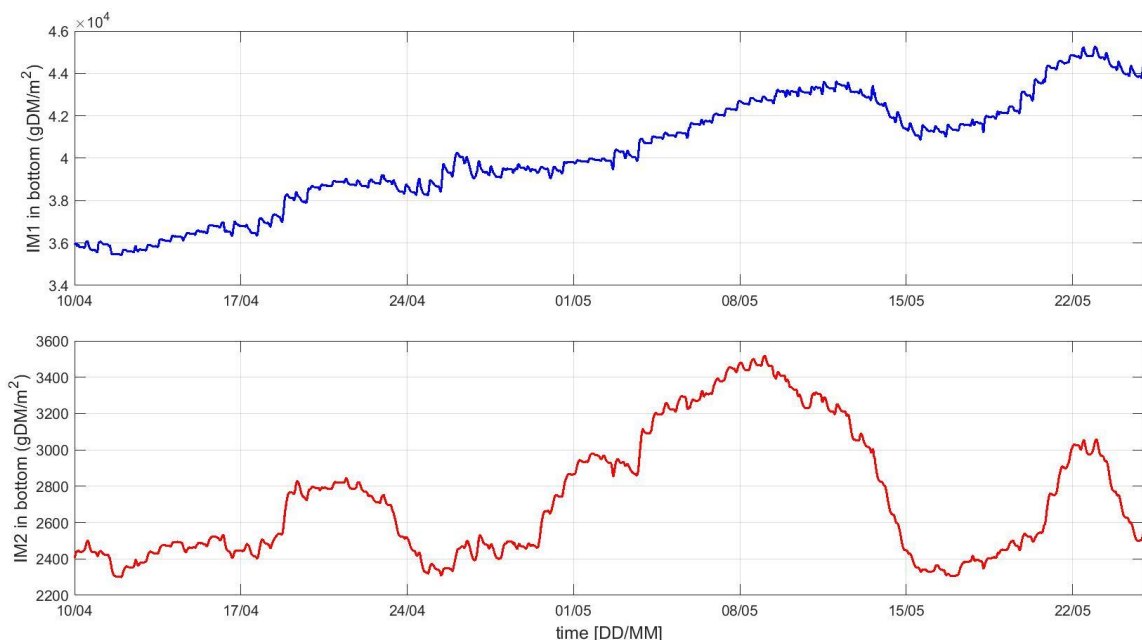

Figure 3.21 Amount of sediment in the bed (S1 and S2) during the first 45 days of simulation 2 (including disposal) for IM1 (top) and IM2 (bottom).

4 Conclusions and recommendations

4.1 Conclusions

- Fine sediment transports at the Mud Motor site are strongly influenced by the sediment properties. The coarser fraction in this study, (i.e. with a settling velocity of 1.5 mm/s) has more interaction with the sediment bed and is therefore sensitive to wave-driven resuspension and tidal asymmetries. This results in a transport from the Mud Motor disposal site in north-eastern direction (i.e. towards the Koehoal mudflat). The finer fraction in this study (i.e. with a settling velocity of 0.2 mm/s) has less interaction with the sediment bed and is therefore more influenced by the residual flow, which is in the Kimstergat channel generally directed towards the southwest. This fine fraction only settles in very sheltered areas, like for example in the Port of Harlingen.
- Residual fine sediment transport varies strongly with the wind conditions and increases with wind speed. The residual flows are also varying with the wind conditions. This behaviour is reproduced but underestimated in the model because of underestimation of the flow velocities at the tidal flats.
- The coarser sediment is transported partly directly to the Koahoal mudflat, and partly to the tidal flats north of Koehoal, from where it is transported to Koehoal again. This seems to be a very local recirculation pattern.
- The sediment from the Mud Motor disposal location is hardly transported over the local tidal divide at the Terschellinger Wad on the time scales that are considered in this modelling study (i.e. approximately one year). Large suspended sediment fluxes that have been measured by Colosimo et al. (in review) at the study site might originate from elsewhere or are very locally resuspended (i.e. at the Koehoal mudflat).
- Approximately 10% of the disposed sediment of the coarser fraction that is transported in flood direction is settling at the Koehoal mudflat. If the coarser fraction (and not the finer fraction!) is representative for the sediment disposed at the Mud Motor location, this would imply that the sedimentation thickness of the disposal at the Koehoal mudflat is approximately 1.5 cm (when consolidated). This is in line with estimations from the tracer experiment and smaller than the LiDAR vertical accuracy and an order of magnitude smaller than the natural sediment dynamics in the area. In the LiDAR surveys we did also not detect sedimentation as a result of the Mud Motor, which is in line with the model results. Note that the model results are sensitive to the sediment properties (different effectivity of the Mud Motor for different settling velocities).

4.2 Recommendations

- The success of the Mud Motor project can be assessed in more detail by further developing the current model, that unfortunately has become available only shortly before the end of this project. The effect of different disposal strategies for the Port of Harlingen is an application that would be useful in the light of the Mud Motor project.
- For most fine sediment projects in the Wadden Sea and the Ems estuary a spin up bed sediment distribution is required, so the results are not influenced by the sediment availability as in this study.
- As the sediment transport in the Wadden Sea is very sensitive to the settling velocity (i.e. residual transports in opposite directions for the two fractions in this study), further fine sediment transport studies should choose the sediment properties carefully and based on sensitivity tests and validation with fields observations. These sediment properties include critical shear stress for erosion, erosion rate, burial, deposition efficiency in addition to the already mentioned settling velocity.

- The wave modelling requires further refinement. The Brettschneider wave schematization has proven its value in this study on a small spatial scale. It might be a runtime efficient solution for the entire Wadden Sea if the fetch length is made spatially varying, although some of the limitations of the simplified approach would remain (e.g. the fetch length is the same during high and low water levels).
- The current hydrodynamic model should further be calibrated using the limitedly available flow velocity measurements (for example from the Mud Motor and SEAWAD field campaigns).

References

Baptist, M., J. Vroom, P. Willemsen, M. van Puijenbroek, B. van Maren, P. van Steijn, M. van Regteren, I. Colosimo. (2019). *Beneficial use of dredged sediment to enhance salt marsh development by applying a 'Mud Motor': evaluation based on monitoring.* WMT & Deltares report.

Colosimo, I., P.L.M de Vet, D.S. Van Maren, A.J.H.M. Reniers, J.C. Winterwerp, B.C. Van Prooijen. (in review). Tide-Wind Interaction Effects on the Intertidal Flat Sediment Transport. *Journal of Geophysical Research*.

Schrijvershof, R., & L. de Vet. (2018). *Morfologisch modelleren plaatrandstortingen Plaat van Walsoorden.* Deltares report 1230096-000.

Schulz, K., & Gerkema, T. (2018). An inversion of the estuarine circulation by sluice water discharge and its impact on suspended sediment transport. *Estuarine, Coastal and Shelf Science*(200), 31-40.

van Kessel, T. (2015). *Opzet en toepassing slibmodel Waddenzee .* Deltares report 1220102-000.

van Kessel, T., Winterwerp, H., van Prooijen, B., van Ledden, M., & Borst, W. (2011). Modelling the seasonal dynamics of SPM with a simple algorithm for the buffering of fines in a sandy seabed. *Continental Shelf Research, 31*, S124-S134.

Vroom, J. (2015). *Modelresultaten slibverspreiding t.b.v. slibmotor Koehol.* Deltares memo 1209751-000-ZKS-0001.

Vroom, J., B. Van Maren, J. Marsh, A. Cado van der Lelij. (2017). *Effectiveness of the mud motor near Koehoal. Results and interpretion of a tracer study.* Deltares report 1209751-004.

Zijl, F., Irazoqui, M., & Groenenboom, J. (2016). Kustmodellen in D-HYDRO - Advies voor algemeen functioneel ontwerp voor de zesde-generatie modellen van RWS. *Deltares report 1230071*.

A   Appendix

A.1: Residual sediment transport between areas in simulations 2 and 3

This appendix includes six figures that show the cumulative residual sediment transport between observation areas in model simulations 2 and 3. The results illustrated in these figures are discussed in Chapter 3, albeit in a rather qualitative form.
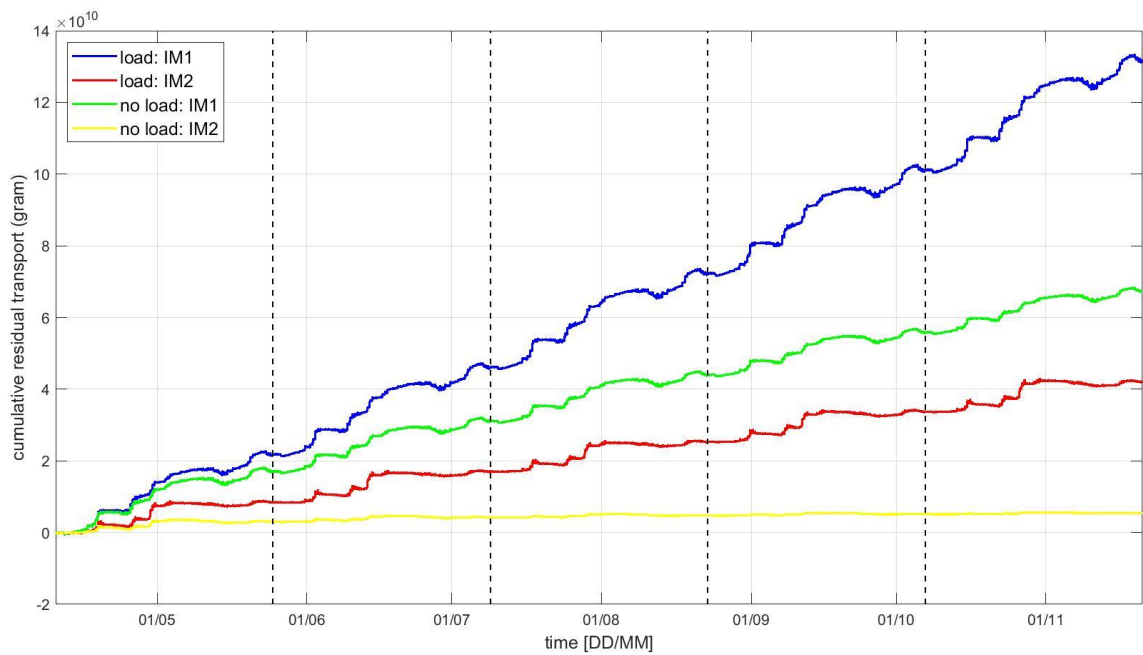

Figure A.1   Timeseries of the cumulative residual transport of IM1 and IM2 from the Kimstergat to Flat_north (see Figure 3.6) in model simulations 2 (continuous disposal) and 3 (no disposal). The vertical dashed lines indicate the five blocks in which the hydrodynamic forcing is repeated.
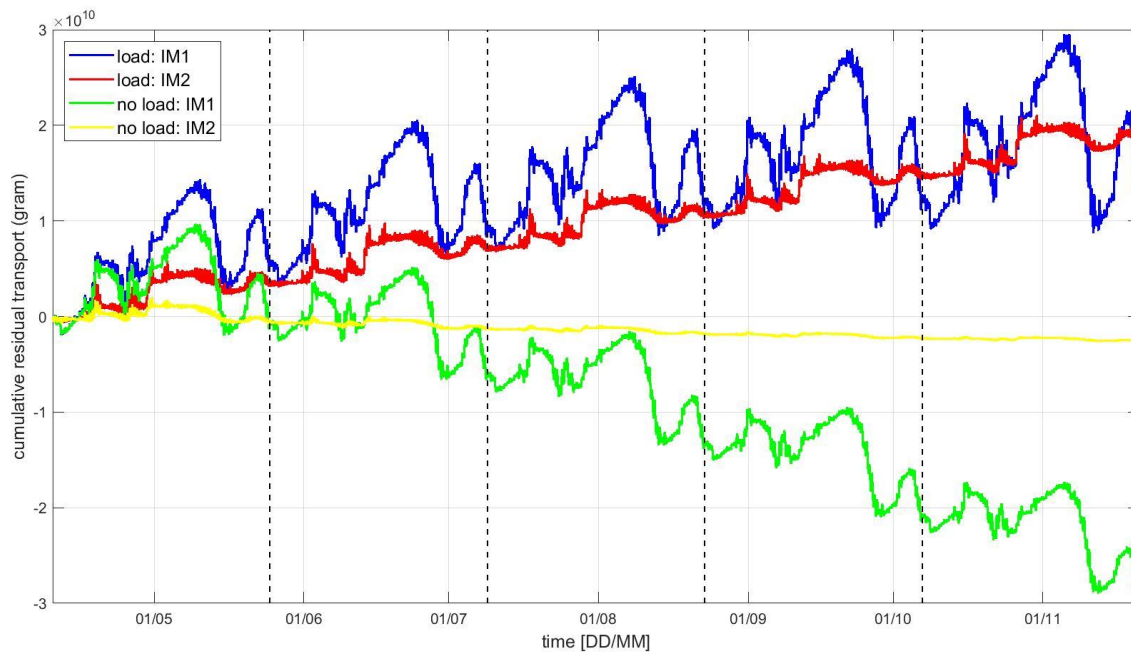
Figure A.2   Timeseries of the cumulative residual transport of IM1 and IM2 from the Kimstergat channel to Flat_frames (see Figure 3.6) in model simulations 2 (continuous disposal) and 3 (no disposal).
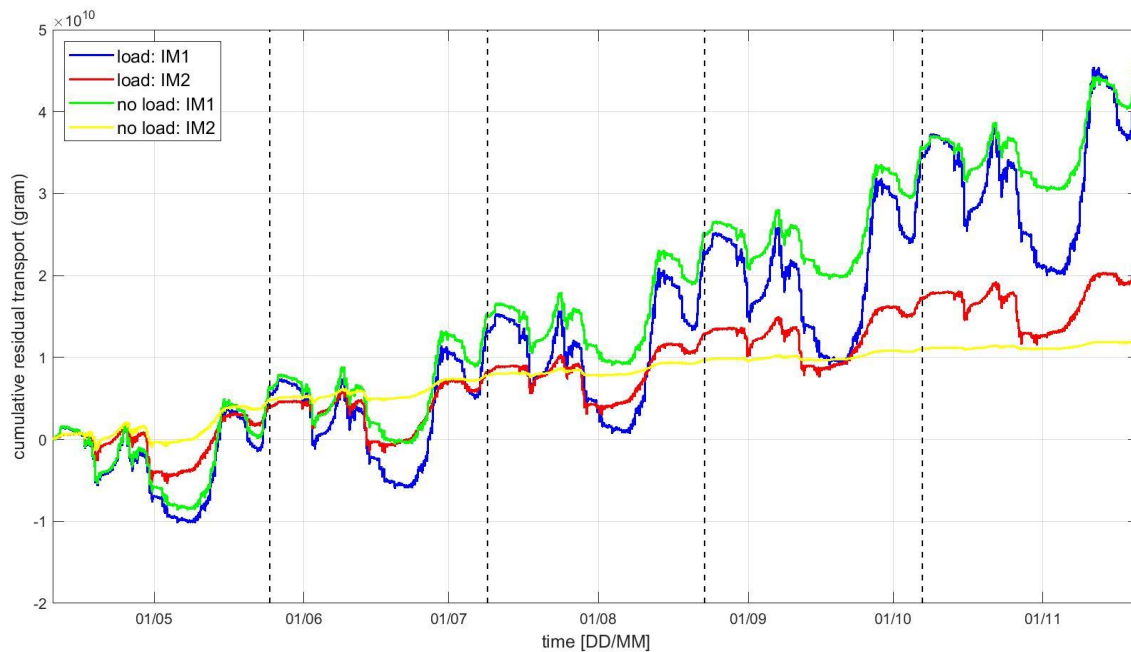

Figure A.3   Timeseries of the cumulative residual transport of IM1 and IM2 from Flat_north to Flat_frames (see Figure 3.6) in model simulations 2 (continuous disposal) and 3 (no disposal).
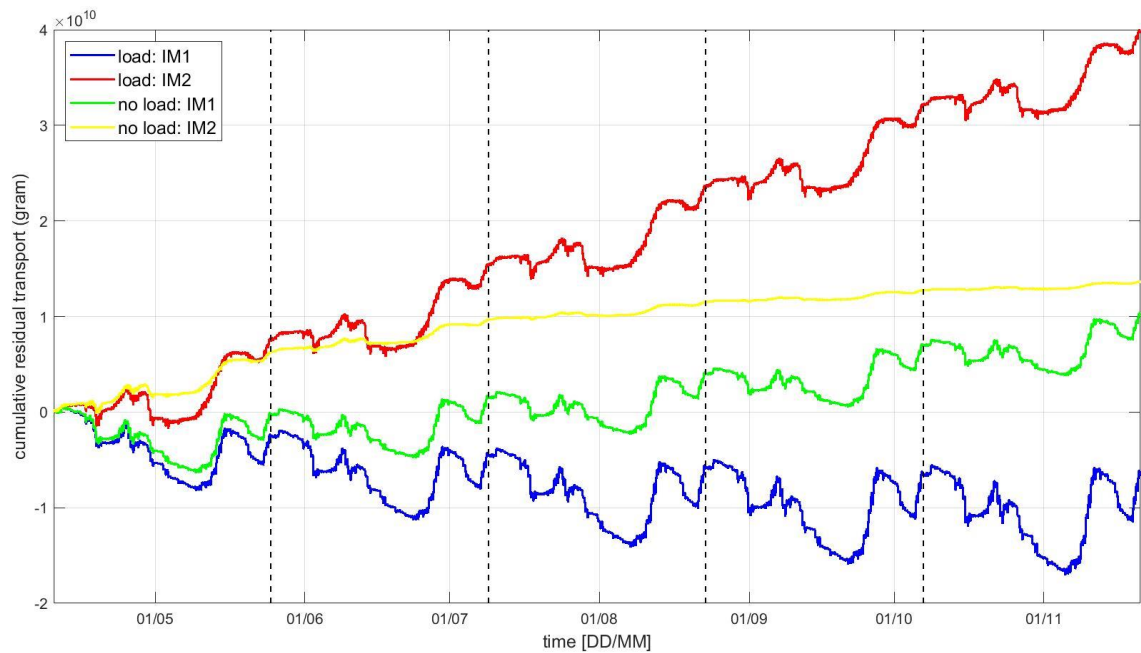
Figure A.4   Timeseries of the cumulative residual transport of IM1 and IM2 from Flat_frames to the coastal stretch south of the channel (see Figure 3.6) in model simulations 2 (continuous disposal) and 3 (no disposal).
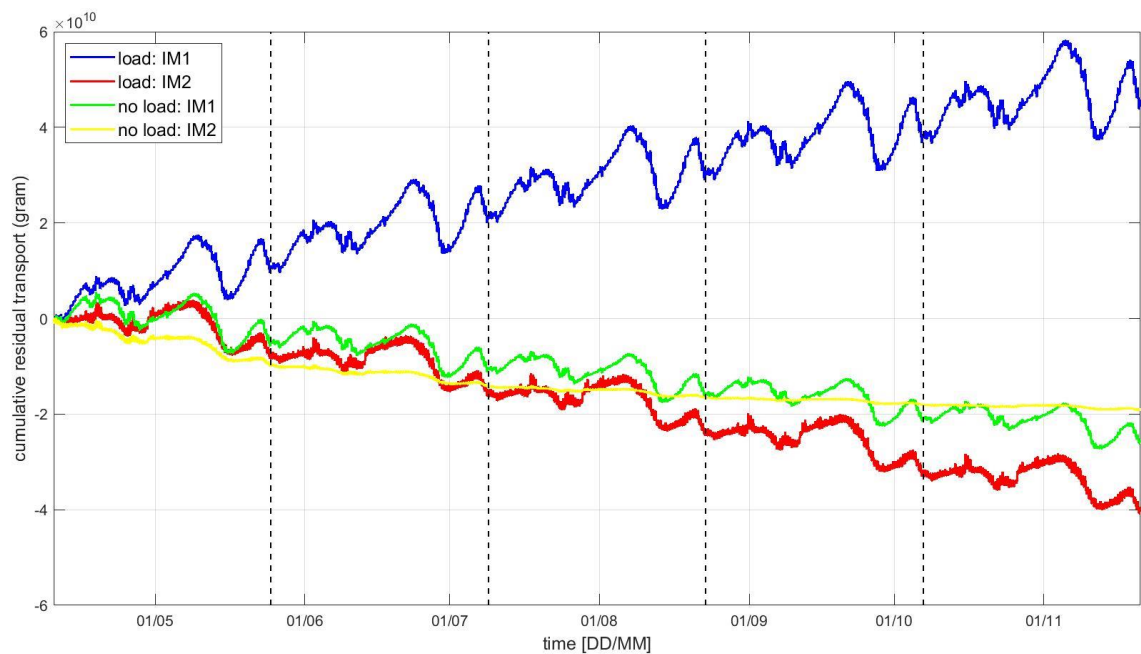

Figure A.5   Timeseries of the cumulative residual transport of IM1 and IM2 from the Kimstergat channel to the coastal stretch south of the channel (see Figure 3.6) in model simulations 2 (continuous disposal) and 3 (no disposal).
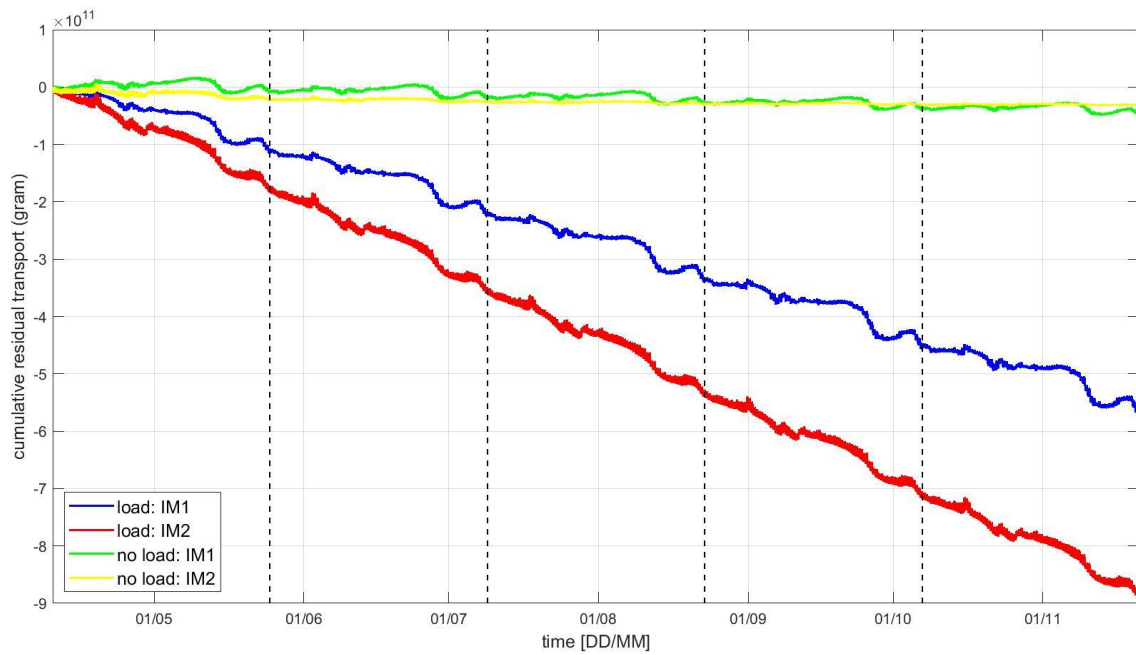
Figure A.6   Timeseries of the cumulative residual transport of IM1 and IM2 from the Kimstergat (1: Kimstergat East) channel towards the west (2: Kimstergat West) in model simulations 2 (continuous disposal) and 3 (no disposal)